QUANTIFYING DROUGHT-INDUCED CHANGES IN GREEN VEGETATION FRACTION AND CLASSIFICATION ACCURACY USING HYPERSPECTRAL DATA FOR THE CENTRAL SIERRA NEVADA, CALIFORNIA

by

Erika Ann Wenrich

A thesis submitted to the faculty of
The University of Utah
in partial fulfillment of the requirements for the degree of

Master of Science

Department of Geography

The University of Utah

December 2017

The University of Utah Graduate School

STATEMENT OF THESIS APPROVAL

The thesis of **Erika Ann Wenrich**

has been approved by the following supervisory committee members:

Philip Dennison	, Chair	**9/22/17**
		Date Approved
Andrea Brunelle	, Member	**9/22/17**
		Date Approved
Mitchell Power	, Member	**9/22/17**
		Date Approved

and by **Andrea Brunelle** , Chair/Dean of

the Department/College/School of **Geography**

and by David B. Kieda, Dean of The Graduate School.

ABSTRACT

Persistent drought conditions and associated vegetation mortality in the central Sierra Nevada of California were analyzed from 2013-2015 using a combination of field-derived polygons and AVIRIS hyperspectral data. Linear Discriminant Analysis (LDA) was used to classify hyperspectral data into 5 land cover classes based on dominant flora. LDA accuracies were compared across years in order to determine whether classification accuracy was correlated with increasing drought severity. It was determined that 2013 had the greatest accuracy and 2015 had the lowest. However, this trend was influenced by Bidirectional Reflectance Distribution Function (BRDF) effects in the densely forested landscape.

Fractional cover data of green vegetation (GV), non-photosynthetic vegetation (NPV), and soil were obtained from the US Forest Service to analyze which land cover classes and which elevation intervals experienced the greatest fractional cover change, which are both indicators of vegetation senescence and mortality. GV loss deemed the most appropriate indicator of vegetation senescence and mortality as NPV and soil appeared to be confused by the Multiple Endmember Spectral Mixture Analysis (MESMA) method used to obtain the fractional cover images. Mixed oak woodland (MO) and mixed low conifer (LC) forests experienced the greatest and second-greatest decreases in GV, respectively. Lower elevation areas (695-1369 m) generally

experienced greater GV loss than higher elevation areas (2167-2779), which coincided with both MO and LC forest classes.

The MO forest class, which occurs most in lower elevation areas, was comprised of dominantly drought resistant flora and experienced the greatest GV loss during the study period (16%). Conversely, the HC forest, which occurs dominantly in higher elevation areas, was comprised of dominantly non-drought-tolerant flora but experienced less GV loss (5%). This suggests that the differences in elevation and location of vegetation within the landscape played a larger role than the dominant floras' degrees of drought tolerance.

Variations in seasonal senescence may have influenced the measured loss of GV for the MO and LC classes, which contained deciduous vegetation. However, overall GV loss in all classes, even those without trees, indicates that the landscape likely experienced vegetation mortality, especially at low elevations in the MO and LC classes.

TABLE OF CONTENTS

LIST OF FIGURES

Figures

ACKNOWLEDGMENTS

There are numerous individuals to whom I would like to extend a sincere thanks for their roles in helping me complete this research. My advisor, Philip Dennison, was instrumental in helping me develop, refine, and complete this research project and has my earnest gratitude. Additionally, I would like to thank Andrea Brunelle and Mitchell Power, my two additional committee members, for their guidance and support throughout the past two years.

I would also like to thank Zachary Tane, Alex Koltunov, and Carlos Ramirez from the US Forest Service Region 5 Remote Sensing Lab for providing me with georeferenced AVIRIS reflectance data. Furthermore, Zachary Tane provided modeled fractional cover data, which were pivotal to this research.

Finally, I wanted to thank my boyfriend, Peter, our cat, Pepper, and our dog, Ellie for their unwavering support.

CHAPTER 1

INTRODUCTION

1.1 Climate in the American West

Climate in the American West is punctuated over time by periods of drought (Brunelle and Anderson, 2003; Cook et al., 2015; Davis et al., 1985; Davis and Moratto, 1988; Heusser et al., 2015; Kleppe et al., 2011; Robeson, 2015). Some drought events may have relatively little impact on the composition of ecological communities, while others can have lasting and severe consequences through elevated forest mortality (Allen et al., 2010). Water deficits associated with drought increase physiological stress directly by reducing moisture availability in the soil and indirectly by amplifying tree susceptibility to pathogen, insect, and fire outbreaks (Allen et al., 2010). Forest die-off due to ongoing drought conditions is attributed to declines in whole-branch hydraulic conductivities and embolisms, which ultimately result in hydraulic failure (Anderegg et al., 2016a, 2014; Choat et al., 2012). Exceptionally warm temperatures during a drought can also serve to worsen its effects by increasing evaporative demand in the soil and leaf canopies (Asner et al., 2015). As global temperatures continue to rise, so does the risk for accelerated forest mortality and community changes, especially for forests within or near water-limited climates such as the mediterranean climate (Cs - Köppen Climate Classification) present throughout California (AghaKouchak et al., 2014; Allen et al.,

2010; Anderegg et al., 2016b, 2014).

1.2 Drought in the American West

The American West is currently affected by a drought which, by one account, first began around 2005 and became a megadrought, in 2015 after 10 consecutive years of persistent drought conditions (Kogan and Guo, 2015) (Figure 1). Megadroughts generally have been defined as droughts that persist for at least 10 consecutive years without alleviation. Although periods of drought are not uncommon within the Western U.S., this most recent event is characterized by a longer duration and elevated temperatures when compared to other drought events within the last 30 years, which typically lasted from 1 to 4 years (Kogan and Guo, 2015). The current drought is therefore the only mega-drought to occur in over 30 years. Drought accompanied by elevated temperatures is associated with vegetation mortality, wildfires, and increased insect attacks (Williams et al., 2010). The likelihood of these hot drought events occurring is increasing in probability and spatial extent, and is exacerbated by the multidecadal length over which these drought events are likely to occur (Overpeck, 2013).

Anthropogenic contributions to a warming climate have served to intensify and worsen the effects observed during this anomalous drought and will increase the likelihood of extreme drought and hydrologic events into the 21st century (AghaKouchak et al., 2014; Cook et al., 2015; Miller et al., 2009; Stewart et al., 2015; Williams et al., 2015). Droughts that extend across entire continents, such as the pan-continental drought of 2012, which occurred in 12% of years during the past millennium, may likely increase in frequency as greenhouse gas emissions increase (Cook et al., 2014). Prediction

modeling shows a 75% probability that the American West will experience widespread megadrought conditions before 2100 under a low CO_2 emission scenario, which increases to an 80-99% likelihood under high emissions (Ault et al., 2016; Cook et al., 2015). Continued monitoring and assessment of forest health and potential risk to ecosystem services during the recent drought is vital for resource managers as well as for climate change prediction modeling.

1.3 Vegetation Response to Drought Conditions

The highest intensity drought and most severely affected area lies within the state of California, which is home to some of the oldest and most diverse forest ecosystems in the U.S., including taxa such as the giant sequoia (Figure 1) (Asner et al., 2015; Belmecheri et al., 2016; Fuchs, 2016). In 2014, ~70% of the vegetation in California was under stronger than moderate stress while 40% of the vegetation in California was under "severe" to "exceptional" stress (Kogan and Guo, 2015). According to the National Drought Mitigation Center (NDMC), exceptional drought conditions may cause exceptional and widespread loss of crop and pasture (Fuchs, 2016). Some of the forest ecosystems in California that are most vulnerable to drought are those located on the west slope of the Sierra Nevada because of their hydraulic-dependence on winter snowpack. Drought conditions there were exceptional even at high elevation and experienced significant canopy water loss due to the recent drought (Asner et al., 2015). These oak woodland and conifer forests are situated topographically above a dry chaparral ecosystem and typically receive precipitation from air masses as they are forced to rise over the crest of the Sierra Nevada to the east.

Mortality, or death, of vegetation can occur in response to multiple circumstances including drought-induced hydraulic failure, fires, disease, bark beetles, and other blights. Recovery of vegetation in a postmortality circumstance also varies due to a variety of conditions including soil moisture, temperature, taxa-type, and topography. Meng et al. (2015) found that for mixed conifer and red fir forests of California, postfire recovery did not fully occur after 5 years. Additionally, greater soil moisture and mild temperatures in the first year following mortality were associated with a more substantial recovery in the fifth year postmortality (Meng et al., 2015). Drought, like fire, can result in 100% vegetation mortality in a given area; however, fire yields different soil-nutrient responses than drought. Postfire recovery times of greater than 5 years may serve as first-order approximations of drought-recovery times. Also, as drought is alleviated, the magnitude of postdrought precipitation and temperatures may affect how quickly vegetation recovers.

1.4 Research Objectives

1.4.1 Goals

The hypothesis of this study is that drought-induced vegetation response is quantifiable via measurement of decreasing fractional photosynthetically active vegetation cover, and is more pronounced at lower elevations; therefore, forest ecosystems that exist at lower elevations have a greater vegetation response to drought than those at higher elevations. Secondary to this is that intense drought conditions in the montane Sierra Nevada forests are correlated with impaired classification accuracy of land cover.

The objectives of this study are twofold; 1) To quantify how Green Vegetation (GV) fraction within certain vegetation types changed from 2013 to 2015 using hyperspectral imagery from the Airborne Visible Infrared Imaging Spectrometer (AVIRIS). This project seeks to understand which forest ecosystems are most impacted in the central Sierra Nevada by identifying where elevated mortality occurs in the landscape, as indicated by a decline in GV fraction. 2) To assess how classification accuracy of each image changes through time on an interannual scale, as classification accuracy may change with mortality. This research will consider the following questions:

1. How do changes in GV fraction compare for different forest types and in which forest class does GV fraction decrease the most? Where is drought-induced mortality occurring in the landscape and is elevation a significant predictive variable?

2. How does classification accuracy change from 2013 through 2015 during the month of June? Is there a relationship between image classification accuracy and change in GV fraction?

1.4.2 Significance

Continued assessment of forest mortality where exceptional drought conditions persist in the lower Sierra Nevada is vital for monitoring and managing forest resources. These results will provide insight to how ecosystems may be changing through mortality under a rapid climate change regime and thus allow for preparedness in making more informed forest and bioecological management decisions, such as selective cutting, habitat management, and access-restrictions, as megadroughts continue into the 21st century. Ultimately, we can begin to understand better how rapid climate change may

influence the degree of forest mortality within different forest ecosystems. Additionally, this study will determine the degree to which changes in forest mortality in response to drought affect image classification accuracy.

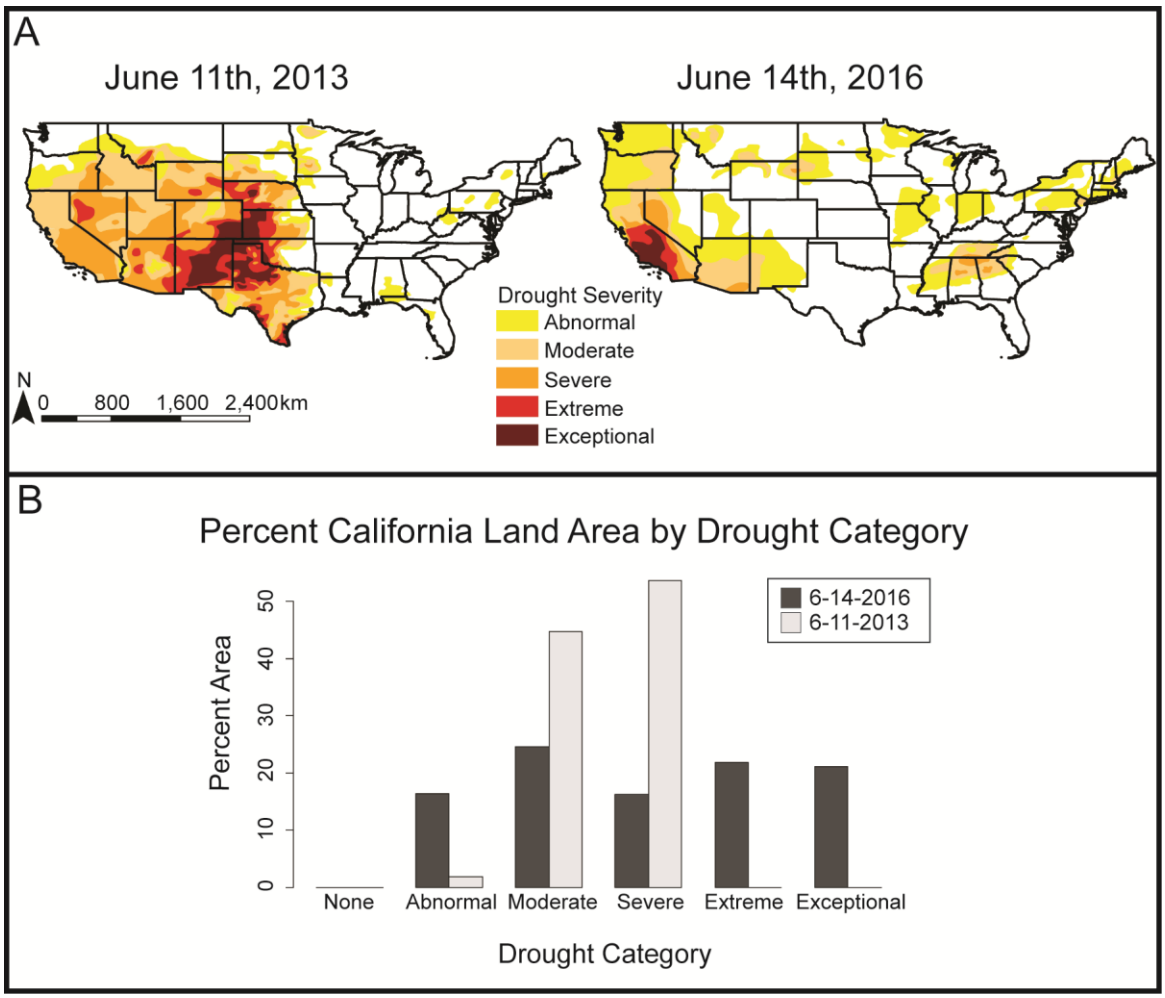

Figure 1. This figure contains a summary of drought conditions in the American West during the study period. A) Exceptional drought conditions occurred across the Midwest during 2013 but were alleviated in this region by 2016. Since 2013, drought conditions have intensified to exceptional status within the state of California and notably over vulnerable forest ecosystems in the central to southern Sierra Nevada. Drought severity increases from abnormal to exceptional and is based on a number of drought indices including the Palmer Drought Severity Index (PDSI). The U.S. Drought Monitor is jointly produced by the NDMC at the University of Nebraska-Lincoln, the U.S. Department of Commerce, the U.S. Department of Agriculture, and the National Oceanic and Atmospheric Administration. Map data are courtesy of NDMC-UNL. B) Bar graph summarizing the percent land area in the state of California by drought category for June 11th, 2013 and June 14th, 2016. Within the state of California for 2013, all land area fell within abnormal, moderate, or severe status but by 2016, drought conditions intensified to include extreme and exceptional status (Fuchs, 2016).

CHAPTER 2

BACKGROUND

2.1 Drought Severity and Preliminary Forest Assessment

Although drought is common for California, few studies have modeled predicted vegetation change in response to drought stress for the Sierra Nevada region (Dolanc et al., 2013) and the potential impact of the drought on vegetation mortality remains poorly understood. However, in a study analyzing growth-climate relationships for six common species of trees in the Sierra Nevada, snowpack was found to be a significant variable for predicting growth trends (Dolanc et al., 2013). Trees growing where snowpack is deep during the wet season are least likely to suffer from drought stress, although it was determined that drought stress was already present within the region and snowpack is predicted to decrease by 30-90% toward the end of the 21st century (Dolanc et al., 2013). Vegetation response to increasing drought stress is likely to vary according to species and lag, out of equilibrium, behind a rapidly warming climate (Dolanc et al., 2013). Flora with sufficient reserves of energy will not begin to show drought-related senescence until these reserves are sufficiently depleted; the amount of reserved energy and duration of lag is thus dependent on both environmental circumstances and species-dependent drought tolerance. Vegetation in southwestern regions of the Sierra Nevada with high ozone concentrations is even more susceptible to stresses associated with climate change,

especially at elevations below 2,400 m (Panek et al., 2013). On geologic time-scales, Töpel et al. (2012) analyzed the fossil Rosaceae and determined that drought stress may have induced plant diversification through adaptation in the American West ~23 Ma. Diversification sometimes occurs during drought events possibly because taxa that are normally dominant in ordinary environmental conditions are not necessarily able to out-compete other taxa for resources, which may allow an array of normally minority taxa to successfully compete for those resources. Additionally, if minority taxa achieve high abundances within the landscape through successful competition, these taxa's pollen, which normally is not likely preserved in ordinary environmental circumstances due to low abundance, may be more likely to be preserved during drought. For vegetation prediction modeling, community composition change as a long-term response to drought could prove to be an important variable.

A recent study used blue oak tree ring data to calculate Snow Water Equivalent (SWE) across the entire Sierra Nevada mountain range in California over the past 500 years (Belmecheri et al., 2016). SWE is an important gauge because most of California's precipitation accumulates as snow, which later melts and becomes the primary water source (AghaKouchak et al., 2014). In 2015, the Sierra Nevada experienced the lowest SWE in 500 years, at 5% of its historical average (Belmecheri et al., 2016). This anomalously low SWE event had a calculated recurrence interval of ~3,000 years even though drought events of a similar severity occurred during the 16th century, highlighting the extreme nature of this low precipitation event (Belmecheri et al., 2016). The 2015 SWE value exceeded the 95% confidence interval from a model defining a 1,000 year recurrence interval (Belmecheri et al., 2016). This period of record low precipitation for

California also coincided with record high temperatures. March, 2015 was ~4°C above the 20th-century average (NOAA, 2015), exacerbating the effects of low precipitation on drought severity (Mao et al., 2015), especially in the lower elevation Sierra Nevada (Belmecheri et al., 2016).

Cook et al. (2015) modeled climate change projections across western North America and calculated changes in drought severity using the relative Palmer Drought Severity Index (PDSI) and compared these projections to similar periods of megadrought during the Medieval Climate Anomaly (MCA). These models showed a significant increase in drought severity during the second half of the 21st century when compared to droughts during the 20th century and MCA (Cook et al., 2015). June PDSI values were calculated for a 122-year precipitation record at a station in Yosemite National Park (YNP), in the central Sierra Nevada (Figure 2). Two-tailed z-score analysis on the PDSI time series shows that 2014 and 2015 had different PDSI values from most of the population (Figure 2). Droughts across the American West are projected to "exceed even the driest centuries of the Medieval Climate Anomaly" in both moderate and severe future carbon dioxide emission scenarios (Cook et al., 2015). In other words, the current megadrought observed in California is likely the beginning of a series of more extreme droughts, which may not be comparable to past drought intervals within existing sedimentological paleoclimate records.

The USDA conducted an aerial survey in May of 2016 over the Sierra Nevada foothills, Transverse, and Coastal Ranges and reported that 876,000 acres had elevated conifer forest mortality out of the 4.5 million acres surveyed (USDA Forest Service, 2016). This exceptional drought event is causing widespread forest mortality, most

severely within oak woodland and mixed conifer forests located along the west slope of the southern Sierra Nevada mountain range in California. Conifer mortality was especially severe within the southern Sierra Nevada foothills and the most affected species were identified as ponderosa pine, Jeffrey pine, sugar pine, white fir, incense cedar, and various oak (USDA Forest Service, 2016). Although visual monitoring of forests offers the advantage of immediate assessment, remote sensing methods remain superior for capturing the large and continuous portion of the landscape in order to detect heterogeneous impacts of drought on forest mortality. For example, one method of visual monitoring, referred to as aerial sketch mapping, was analyzed using data from 2005 for accuracy and determined to have a maximum accuracy of 79% at a 500 meter scale and a minimum of 61% at a sub-meter scale, which is not acceptable for most quantitative studies (Johnson and Ross, 2008).

2.2 Hyperspectral Remote Sensing

2.2.1 Hyperspectral vs. Multispectral

Data from broadband sensors (e.g. Landsat, SPOT, etc.) contain a small number of spectral channels, or bands, with wide bandwidths (typically 30-100 nm). In contrast, imaging spectrometers retrieve upwelling radiance data for potentially *hundreds* of narrow spectral bands (~10 nm), or channels, over a contiguous portion of the electromagnetic spectrum. Images produced by imaging spectrometers are referred to as hyperspectral, in contrast to multispectral data obtained by broadband sensors. Contiguous spectra measurements from hyperspectral sensors offer unparalleled advantages in determining the composition of materials on Earth's surface over data

obtained from multispectral sensors. Accuracy assessments show that hyperspectral data vastly outperform their broadband counterparts in measuring vegetation variables (Asner and Heidebrecht, 2002; Keshava and Mustard, 2002). Hyperspectral data have high spectral fidelity and allow for sub-pixel discrimination of different materials on Earth's surface, the identification of different plant species, and a better estimation of different biophysical, biochemical, and structural parameters across various vegetated ecosystems (Asner et al., 2008; Behmann et al., 2014; Chen et al., 2008; Dennison and Roberts, 2003a; Dudley et al., 2015; le Maire et al., 2008; Thenkabail et al., 2004a, 2004b). Additionally, these relatively new spectrometers have allowed for earlier detection of changes in reflectance for vegetation canopies due to changes in the environment from climatic perturbations such as drought (Asner et al., 2015; Behmann et al., 2014; Coates et al., 2015).

2.2.2 Hyperspectral for Discriminating Species and Land Cover Types

Hyperspectral data offer the advantage of near-continuous spectra, enabling researchers to obtain more accurate classification results for plant communities when compared to those obtained from broadband analyses (Thenkabail et al., 2004a). Chemical and physical attributes unique to different species of trees affect the spectral signatures of canopies, and variations of these attributes allow investigators to differentiate and classify canopy species via these distinctive spectral signals (Asner, 1998). Several studies have utilized hyperspectral data for species-level classification based on spectral variability within forest communities (Beland et al., 2016; Cochrane, 2000; Roberts et al., 2015; Roth et al., 2015a) as well as for invasive species detection

(Asner et al., 2008). The integration of waveform Light Detection and Ranging (LiDAR) data has also been shown to increase forest classification accuracy when coupled with hyperspectral imagery (Anderson et al., 2008). The degree to which classification accuracy changes with seasonal drought conditions is dependent on the method of classification (Dennison and Roberts, 2003a; Dudley et al., 2015).

2.2.3 Hyperspectral for Measuring Fractional Cover

Roberts et al. (1993) describe green vegetation (GV) as vegetation that contains significant abundances of chlorophyll, such that its spectral reflectance shows high NIR to red spectral contrast, distinguishing it from soil. Non-photosynthetic vegetation (NPV) is defined as vegetation that does not contain significant abundances of chlorophyll such that the reflectance does not have a high NIR to red spectral contrast (Roberts et al., 1993). In some cases, NPV can be spectrally indistinguishable from soil, but with proper calibration and endmember spectral profiles, it is possible to differentiate GV, NPV, and soil in spectral image analyses (Roberts et al., 1993). Studies show that hyperspectral data are valuable for extracting fractional measurements of GV, NPV, and soil when utilizing bands in the shortwave infrared 2 (SWIR2) region (2.0 - 2.3µm) (Asner and Heidebrecht, 2002) and for detecting small differences in percent GV cover (Chen et al., 2008). Such studies are important for fractional vegetation classification of images, which is a component of this study in examining drought conditions in the central Sierra Nevada.

2.2.4 Spectral Unmixing Techniques

Remote sensing systems are designed to measure spectral radiance within a sensor's ground instantaneous field of view. Radiance data are converted into apparent surface reflectance by performing a series of corrections to eliminate non-surface-related signals. A measured spectrum for any given pixel represents combined reflectance for all surficial materials contained within the sensor's field of view. Materials may have their own unique spectral reflectance signature, which is referred to as an endmember. Endmembers are pure spectral reflectance measurements for materials of a known composition and can either be obtained through field observations and imagery, or with lab spectrometers (Dennison and Roberts, 2003b). This combined spectral profile is the result of "spectral mixing" which occurs on micro- to macroscopic scales in the landscape.

The goal of spectral mixture analysis (SMA) techniques is to deconstruct each spectrum within an image into its endmember constituents and estimate the sub-pixel composition of surficial materials. Spectral libraries contain the pure endmember spectra to be used as a reference during the classification process. In some cases, spectral libraries are created by extracting spectra from images within polygons where land cover type is known. SMA models spectra as the linear combination of endmembers from a spectral library, typically using the same set of endmembers for all spectra in an image. A milestone application of SMA was used in modelling the Martian rock and regolith cover adjacent to the Viking 1 Lander using shade and secondary illumination as endmembers (Adams et al., 1986).

2.2.4.1 Multiple Endmember Spectral Unmixing Analysis (MESMA)

Multiple Endmember Spectral Mixture Analysis (MESMA) is a more complex variant of SMA that allows for linear combinations of endmembers to be modeled on a per-pixel basis (Dennison and Roberts, 2003b; Dudley et al., 2015; Roberts et al., 1998). MESMA's utility is that the number and the types of endmembers can be varied across an image, allowing a model to more precisely classify varied, complex ground cover than standard SMA (Roberts et al., 1998). MESMA has been used to estimate the fractional coverage of GV, NPV, soil, and shade with improved accuracy compared to SMA (Roberts et al., 2015).

Root Mean Square Error (RMSE) is calculated for both SMA and MESMA in order to determine the best fitting spectral mixing model for each pixel, using the defined endmembers. For a given pixel, the best fit spectral mixing model with the lowest RMSE is chosen to determine the fractions of each class within the pixel. RMSE is calculated by summing the squares of band residuals, dividing this sum by the number of bands, and then taking the square root (Roberts et al., 1998).

A number of studies have utilized SMA in order to quantify drought-induced vegetation responses (Coates et al., 2015; Elmore et al., 2006; Huang and Anderegg, 2012). Researchers examined the effects of drought on the Santa Barbara Coast and Santa Ynez Mountain area in California for 2013-2014 using SMA models (Coates et al., 2015). As drought conditions persisted, there was a mixed vegetation response where deep-rooted vegetation experienced less fractional GV decrease than shallow-rooted vegetation. In Colorado, researchers utilized a form of SMA in order to quantify the health of aspen forests in 2011 using a three endmember unmixing model (Huang and

Anderegg, 2012). This study quantified drought-induced aboveground biomass loss using NPV as an indication that a forest had undergone dieback as a result of drought.

2.2.5 Linear Discriminant Analysis (LDA) for Hyperspectral Data

Discriminant analysis is one statistical procedure used to classify hyperspectral data using a set of known training, or reference, spectra (Roth et al., 2015b). Discriminant analysis techniques are essentially used to statistically define each pixel as a member of a predefined group or class based on several variables simultaneously. For example, discriminant analysis functions can incorporate spectral information with elevation data or LiDAR in order to more accurately classify a vegetated landscape. The variables used to discriminate between groups of pixels are referred to as discriminating variables. Linear discriminant analyses utilize a linear transformation of data in order to increase the ratio of between-class variance to within-class variance (Roth et al., 2015a). Class discriminant functions are calculated for each class, and spectra are assigned scores for each class. Spectra are then assigned to the class that yields the highest score. LDA techniques have been used to differentiate species-level differences using hyperspectral data, reaching very high classification accuracies (Feret and Asner, 2013; Roth et al., 2015a, 2015b).

2.3 Historic Vegetation Change in the Central Sierra Nevada Due to Drought

2.3.1 Paleoenvironmental Reconstructions of Sediment Core Studies

Researchers have conducted a variety of paleoenvironmental studies utilizing pollen as a proxy for vegetation abundance within a watershed or region in order to detect

long-term responses to variable climate, particularly within the central Sierra Nevada (Anderson and Stillick Jr, 2013; Brunelle and Anderson, 2003; Heusser et al., 2015; Petel, 2005; Smith and Anderson, 1992; Street et al., 2012). Studies that utilize pollen abundances preserved in sediment cores assume sediment records provide a representative sample of surrounding vegetation type over time, which is validated by comparing modern pollen surface samples to modern vegetation composition surveys (Minckley et al., 2008; Petel, 2005). In addition to pollen, sediment cores also record fire occurrences, including those during the MCA and a period known as the early-Holocene Insolation Maximum. Brunelle and Anderson (2003) analyzed charcoal abundances in sediment core from Siesta Lake in Yosemite National Park in order to treat fire events as a proxy for periods of drought across the Holocene. The early-Holocene Insolation Maximum is likely to have had conditions similar to the modern, and researchers have thus suggested a possible 2-4°C increase in average temperature over the next ~90 years (Leung and Ghan, 1999). Comparison of drought events within the Sierra Nevada indicates that the MCA and Insolation Maximum events were more severe than those over the last ~1,000 years (Brunelle and Anderson, 2003). These past trends suggest that as modern global temperatures continue to rise and relative available soil moisture decreases in the Sierra Nevada, drought and subsequent fire events will increase both in frequency and magnitude.

The timing and duration of drought events affect vegetation response, and may cause shifts both in abundance and spatial distribution of flora (Wathen, 2011). Abrupt climate changes occur on the order of years to decades and have punctuated more gradual climate change fluctuations; abrupt changes may have more acute impacts on ecosystems

than gradual ones (Wathen, 2011). During the late Holocene, a climate warming period caused disequilibrium vegetation response within the Sierra Nevada (Wathen, 2011). The MCA was one of the most significant periods of drought for the Sierra Nevada region and occurred from ~900-1200 AD (Kleppe et al., 2011; MacDonald et al., 2008; Millar et al., 2006). During the MCA, forest fires became more frequent (Brunelle and Anderson, 2003) and the treeline shifted upwards in elevation (Millar et al., 2006) with the onset of mountain glacial retreat (Anderson and Stillick Jr, 2013). This period of extended drought and average temperature deviations of ~0.5˚C provides an important benchmark in the paleorecords for comparison with the modern megadrought phenomenon across the American West (Graumlich, 1991).

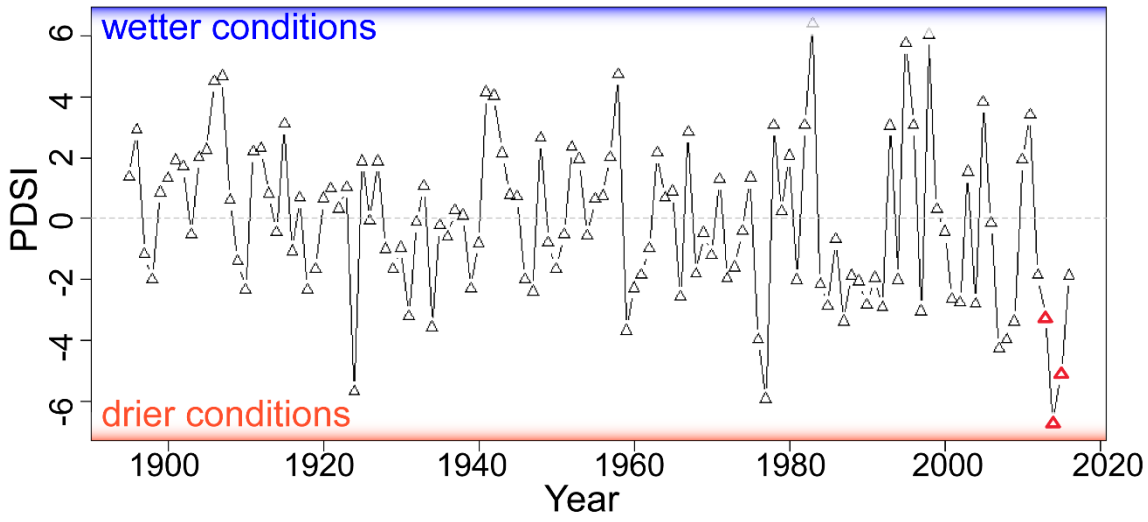

Figure 2. Time-series graph of June Palmer Drought Severity Index (PDSI) values from 1895-2016 for a station in Yosemite National Park, central Sierra Nevada region. Each triangle denotes June PDSI value for given year. Red triangles indicated study period of 2013-2015. PDSI values for the study period range from moderate to extreme drought conditions, which are consistent with conditions during this time throughout much of the Sierra Nevada.

CHAPTER 3

STUDY AREA AND DATA

3.1 Study Area

3.1.1 Topography

The Sierra Nevada Mountains run 640 km in a north-south orientation and stretch ~110 km wide between the Basin and Range province to the east and the Great Valley province to the west (Figure 3). The Sierra Nevada Range is characterized by a gently sloping western margin, which varies in elevation from 300 m near the Great Valley up to an average elevation of 3,200 m at the Sierran crest. The eastern margins slope steeply away from the crest of the range, forming the Sierra Escarpment, and causing a rainshadow over the eastern foothills.

3.1.2 Precipitation

Yearly-averaged precipitation differs slightly from ~1,050 mm in lower montane areas (~1,500 m) to ~1,400 mm at 2,000 m in elevation and gradually declines eastward from 2,000 m (Fites-Kaufman et al., 2007). Temperature does, however, fluctuate considerably across such a large elevational gradient. Generally for the Sierra Nevada, the fraction of precipitation occurring as snow greatly increases with increasing elevation. In the lower forested areas, 20% to 25% of precipitation falls as snow, compared to 95%

or greater accumulating as snow near the upper treeline (Stephenson, 1988). Lower temperatures and deeper snowpack at high elevation (2167-2779 m) allow for a longer period of snowmelt that begins later in the year when compared to melt at lower elevations (695-1369 m). Each of these contributing factors results in relatively lower moisture stress for vegetation at high elevation when compared to vegetation at lower elevation within the Sierra Nevada. Precipitation in California follows a seasonal, winter-wet regime with most precipitation falling during January, February, and March. Summers are exceptionally dry with the least amount of precipitation received during June, July, and August.

3.1.3 Vegetation Zones

Local topography is highly variable and, when coupled with the overall climatic gradient from east to west across the range, largely determines the vegetative composition observed across the landscape. Mixed conifer forests for the montane region may be broken into two broad categories based on relative elevation, both of which lie above mixed oak woodland and drier chaparral-dominant ecosystems: 1) Low montane vegetation, and 2) High montane vegetation. The lower montane forests can broadly be referred to as Sierran mixed-conifer forests and are dominantly comprised of ponderosa pine, blue oak, and white fir. About 30% of precipitation within this vegetative zone falls as snow (Fites-Kaufman et al., 2007). Upper high montane forests grow at elevations above the mixed-conifer forest types. This transition from lower to upper montane forests occurs around ~1,800 m in elevation for the central regions of the Sierra Nevada (Fites-Kaufman et al., 2007; Smith and Anderson, 1992). Between 70% to 90% of precipitation

in this zone falls as snow and the deepest, longest-lasting snowpack accumulates in this zone when compared to any other area of California (Fites-Kaufman et al., 2007). Red fir, lodgepole pine, and Jeffrey pine comprise the three major conifer forest types within the upper montane zone (Fites-Kaufman et al., 2007). Vegetation composition and forest type classifications vary by location between eastern and western slopes and with the north-south strike of the Sierra Nevada range.

3.2 Data

3.2.1 Digital Elevation Model (DEM)

The USGS maintains a seamless elevation raster product of the continental United States, Alaska, Hawaii, and island territories referred to as the National Elevation Dataset. A set of NED DEM data tiles of the study area were available through a legacy website in GEOTiff format at https://www.mrlc.gov/viewerjs/.

3.2.2 AVIRIS Reflectance Data

Hyperspectral data collected by the Airborne Visible/Infrared Imaging Spectrometer (AVIRIS) contain 224 contiguous, 10 nm wide spectral channels ranging from 350 to 2500 nm (Green et al., 1998). AVIRIS acquires imagery at an altitude of approximately 20 km on an ER-2 aircraft and produces individual scenes that measure 11 km wide by up to 800 km long with a spatial resolution of ~20 m (Green et al., 1998). NASA's Jet Propulsion Laboratory preprocessed all images to terrain corrected reflectance and the Forest Service (Tane, 2016) improved image orthorectification.

Hyperspectral images collected by AVIRIS for 2013 during the month of June

were used to create an initial classified image by land cover type. For 2013, 6 separate scenes were mosaicked, or "stitched together", to create one, spatially contiguous image with some degree of overlap between scenes. Similar reflectance mosaics for 2014 and 2015 were used to classify land cover and produce a final classification accuracy assessment.

3.2.2.1 Fractional Cover Images

A 16 endmember library was used to define GV, NPV, soil, and shade cover fractions using MESMA within ENVI. Endmembers were derived from AVIRIS Next Generation (AVIRIS-NG) data, which measure spectra from 380 nm – 2510 nm at 5 nm spectral resolution across 481 bands. Specifically, endmembers were collected from AVIRIS-NG summertime flights over the Shaver Lake area in 2014 and convolved to AVIRIS wavelengths. An IDL extension for ENVI called VIPER Tools (www.vipertools.org) was used to process 177 bands. MESMA was conducted using an uncorrelated Stable Zone Unmixing method (uSZU) yielding 18 bands that maximized signal-to-noise ratio for endmember profile selection (Somers et al., 2010; Tane, 2016). MESMA analysis was conducted on AVIRIS reflectance data by the U.S. Forest Service for 2013, 2014, and 2015 to produce fractional images (Tane, 2016). All remote sensing data products used in this study are produced from imagery acquired on the dates listed in Table 1.

3.2.3 Field Polygon Survey

A set of 141 polygons was created in 2013 by conducting a field survey within a portion of the central Sierra Nevada. Of these 141 polygons, 122 were selected for use in classification analysis (Figure 4). Primary field observations with aerial imagery ensured that each polygon contains only one type of forest class. The original polygon dataset consisted of 9 land cover classes and, for this study, were reduced to 5 classes (Table 2). The final land cover classes are as follows: Mixed Oak Woodland (MO), Lower Mixed Conifer (LC), High Conifer (HC), Meadow (MD), and Rock (RO) (Table 2). Metadata for each class of polygons contains a description of the dominant vegetation species. Polygons from this dataset were split into validation and reference groups so that each group has a random spatial sample and contains a similar number of pixels for each class.

Table 1. Dates of June AVIRIS data collection for central Sierra Nevada study area by year.

Image Year	Date of Collection
2013	June 6, June 12, June 24
2014	June 3
2015	June 1

Table 2. Class codes, names, and descriptions used for land cover classification of AVIRIS reflectance data. Field polygon work reported that the following vegetation compositions are generally observable on elevation gradients from <300 m to >2100 m in the central Sierra Nevada, in order from lowest to highest elevation: 1) Mixed Oak Woodland, occurring at relatively low elevations; 2) Lower Mixed Conifer; 3) High Conifer; 4) Meadow also occurs in Lower Mixed Conifer and High Conifer regions but is found more often at higher elevations; 5) Rock occurs at various elevations but is found most frequently at higher elevations (Figure 4). These classifications are based on classification of discrete areas.

Class Code	Full Name	Description
MO	Mixed Oak Woodland	Includes: **Mixed Oak Woodland** - >50% shrub and tree cover; species include interior live oak (*Quercus wislizeni*), whiteleaf manzanita (*Arctostaphylos viscida*), buckeye (*Aesculus*), curl-leaf mountain mahogany (*Cercocarpus*), California black oak (*Quercus kelloggii*), Jeffrey pine (*Pinus jeffreyi*), and Oregon oak (*Quercus garryana*). **Grassland** - Low elevation pasture, open, with <10% oak cover. **Oak Savana** - >50% tree cover, blue oak (*Quercus douglasii*) dominated. **Shrub** - Found at similar elevations as MO and less often, lower extent of LC, on dry south or west-facing slopes. Dominated by woolly leaf ceanothus (*Ceanothus tomentosus*) and whiteleaf manzanita (*Arctostaphylos viscida*) taxa, with small percentages of oak and pine possible.
LC	Lower Mixed Conifer	Jeffrey pine (*Pinus jeffreyi*), ponderosa pine (*Pinus ponderosa*) common at lower extent; incense cedar (*Calocedrus decurrens*), California black oak (*Quercus kelloggii*), sugar pine (*Pinus lambertiana*), white fir (*Abies concolor*), ponderosa pine (*Pinus ponderosa*) common at upper extent; giant sequoia (*Sequoiadendron giganteum*) possible, lodgepole pine (*Pinus contorta*) at upper extent.
HC	High Conifer	lodgepole pine (*Pinus contorta*) and red fir (*Abies magnifica*) common, some monotypic stands; ponderosa pine (*Pinus ponderosa*), white fir (*Abies concolor*) also found.
MD	Meadow	Open with few trees, grasses, and herbaceous vegetation.
RO	Rock	Dominated by exposed granitic bedrock usually at high elevation with partial grasses, shrubs and lichen covers.

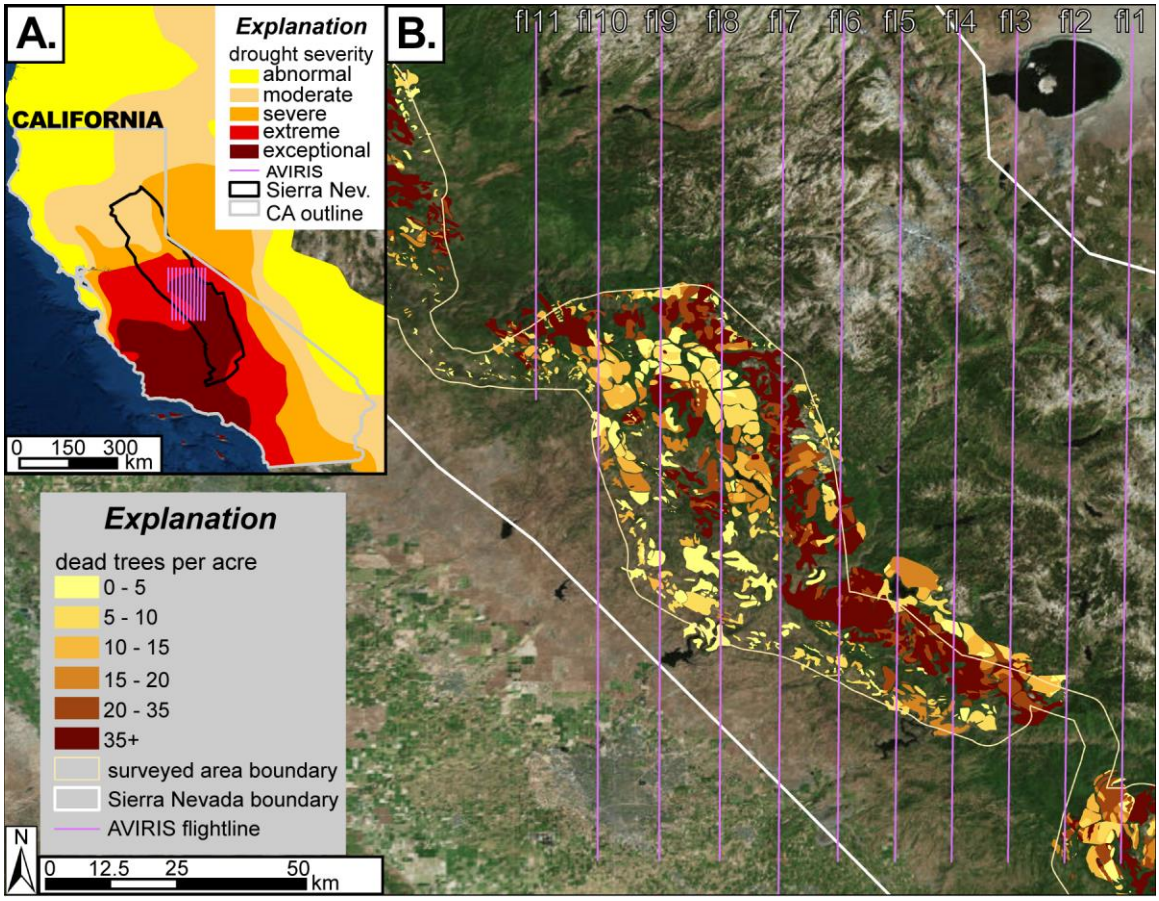

Figure 3. This map illustrates the study area near Fresno, California. A) Inset map of drought severity across California on June 14th, 2016. The Sierra Nevada province is outlined in black and AVIRIS flight lines are outlined in magenta. Exceptional and extreme drought occupy the majority of the Sierra Nevada region. B) Aerial extent of AVIRIS flight lines labeled by flight line number within the Sierra Nevada region with USDA Forest Service dead tree density overlain in color.

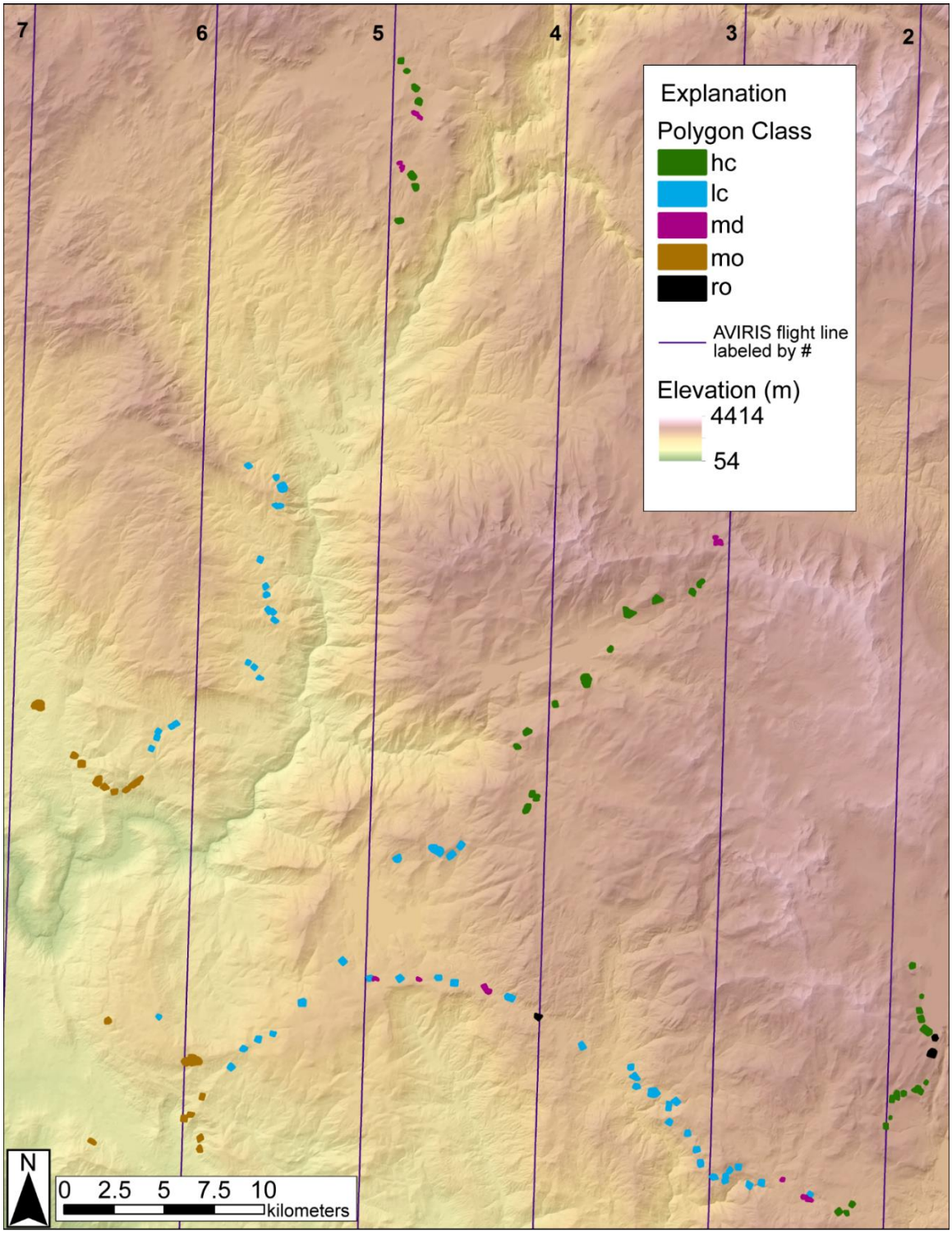

Figure 4. Digital elevation model displayed with low elevations in green to higher elevations in white and hill-shade underlain. Training and validation polygons (n=122) within the AVIRIS flight lines are color coded by the land cover classification types found in Table 2.

CHAPTER 4

METHODS

4.1 Overview

In order to quantify vegetation response to intensifying drought conditions from 2013 to 2015 in the central Sierra Nevada of California, a series of analytical techniques were applied to field collected and remotely sensed data. One method employed was to determine how measureable features such as decrease in GV fraction (as a proxy for vegetation mortality) varied between vegetation classes, across elevation zones, and more broadly across the landscape. As vegetation experiences mortality or senesces, either as a result of drought or other stress-inducing conditions, GV fraction decreases as reflectance increases in the chlorophyll absorption range (400-700 nm) and in both the regions of the shortwave infrared (SWIR and SWIR2) and reflectance decreases in the near infrared (NIR) (Roberts et al., 1993). The decrease of GV and an associated increase in NPV and soil fractions indicates an increase in vegetation mortality and is assumed to occur as a result of vegetation response to drought.

Another method was determining whether vegetation classification accuracy was affected by increasing drought conditions from 2013 to 2015 by comparing assessments of classification accuracy between each year. A lower classification accuracy that coincides with a lower GV fraction in the landscape could indicate that classification

accuracy is negatively affected by vegetation mortality.

All field-derived polygons were assigned into either training or validation polygon groups in order to facilitate subsequent analysis using LDA. The IDL code used for classification was provided by Dr. Philip Dennison and was updated by both Dr. Dennison and Dr. Keely Roth in 2013 and 2015, respectively. Classification of AVIRIS data was conducted in order to map vegetation classes throughout the study area and multiple iterations of classification were conducted for each year's data with minor changes made between runs in order to maximize the classification accuracy for each year. Fractional cover images that were provided by Zachary Tane of the USDA Forest Service were analyzed for changes in values of shade-normalized GV, NPV, and soil, and then were used with existing field polygon data to identify vegetation classes that experienced the largest change in fractional cover.

4.2 Training and Validaton Polygon Categorization and AVIRIS Mosaicking

Supervised classification techniques of spatial data such as LDA require both training and validation sets of polygons for each class. From the 141 field-derived polygons that were delineated in the study area during 2013, two sets were assigned, one of training and one of validation. An important requirement of grouping the polygons was to ensure that for each vegetation class, roughly half of the polygons were put into each set with any remainder being placed into the validation set for a more robust assessment of classification accuracy.

The study area is covered by six individual AVIRIS flight lines that were measured on an annual basis from 2013-2015. Flight lines were mosaicked in ENVI 5.3

Classic using the georeferenced mosaicking tool with a bilinear resampling method. For mosaicked reflectance image results, background values were set to zero, which simplified masking operations. Numerous mosaics for each year were produced to minimize reflectance discontinuities between adjacent flight lines because of differences in solar zenith and azimuth, mosaicked images with smaller reflectance discontinuities yielding the most accurate results.

An overlapped mosaic of AVIRIS flight lines was used to extract training spectra from the training set of field-derived polygons in order to build a spectral library for LDA classification. In areas where overlap between two adjacent flight lines occurred, spectral library extraction would only take into account the top flightline's data, which was delineated by each polygon. This method of training a spectral library from an overlapped mosaic of the entire study area, instead of individual flight lines, yielded the highest accuracy results for 2013 and was consequently utlized for classification of all AVIRIS data.

An alternative method for LDA was attempted, which required dividing all 141 polygons into groups that fell onto individual AVIRIS flight line extents. This method allowed the LDA classifier to train additional spectra for polygons that were located in the overlap areas between two adjacent flight lines, for the flight line data on top and underneath. Once training spectra were collected individually from each flight line, the spectra were combined into a single spectral library and then used to classify the entire study area using a mosaic of all flightlines for a single year. However, this method resulted in lower overall accuracies for classification of 2013 data and was thus abandoned.

4.2.1 Randomization

In order to ensure the unbiased division of polygons for 5 vegetation classes, a table of all field polygons was exported from ArcMap, providing a spreadsheet with unique identification numbers for each polygon. Polygons were divided into separate sheets in Microsoft Excel by all polygons by vegetation class and then cutting and pasting groups of the same vegetation class polygons into separate sheets. For each vegetation class sheet, every polygon was assigned a random number using the "RAND()" function, which generates a random value between 0 and 1. Each sheet was sorted using the randomly assigned numbers to scramble the polygons. Once the polygons were scrambled, they were divided into training and validation polygons by grouping polygons with high random number values together and likewise with low random number values. Thus, for each of the 5 vegetation classes, there were two randomly assigned groups, training and validation for a grand total of 10 groups. Using the ArcMap-generated identification numbers for each polygon, the master polygon shapefile's attribute table was then used to manualy select only polygons from one class, which were then exported as new shapefiles, one training and one validation shapefile. This method was employed in order to randomize the process of selecting training and validation polygons for each of the 5 vegetation classes.

4.3 Linear Discriminant Analysis (LDA)

4.3.1 Bidirectional Reflectance Distribution Function (BRDF) Effects

The AVIRIS data utilized in this study were affected by BRDF effects that caused both anomalously high and low values for reflectance values based on varying view

angles and measured wavelengths. BRDF effects are especially problematic in data with large fields of view (FOV), such as AVIRIS data that has a ~34º FOV. Backscattering is the preferential reflection of light back towards the illumination source causing higher than normal reflectance values. Shadows are the absence of reflected light and occur in areas where surface structure blocks solar insolation, especially during high solar zenith angle periods. If backscattering is recorded on one side of the FOV and/or shadows are recorded on the opposite side, a gradient in reflectance values across the image oriented across the image swath will emerge in the data. A gradient will not likely occur perpendicular to the sensor sweep path because the sensor remains fixed relative to the ground surface between successive sweeps, and thus there are no view angle changes that occur orthogonal to the sweep line.

Reflectance values, even in areas of relatively uniform land cover, differed as a function both of the view angle from which the sensor collected data and the wavelengths that were measured (Figure 5).

Backscattering caused increased reflectance values on flight lines in the direction opposite of solar azimuth relative to the center of the sensor sweep. Conversely, reflectance values in the same direction as solar azimuth relative to the sensor sweep were lower as a result of shadows. Thus, each flight line that was utilized via AVIRIS collection was subject to some degree of these effects on surface reflectance, which caused strong discontinuities between some adjacent flight lines. Manually selecting flight line overlaps to minimize these effects across the image was necessary in order to produce results with sufficiently high accuracy, especially for training and validation pixels used in LDA classification (Figure 5).

4.3.2 Resampling and Layer Stacking

DEM data from the National Elevation Dataset (NED) were obtained for the entire study area at a 10 meter resolution and were resized to the AVIRIS data extent as well as resampled using a bilinear method in ENVI. The mosaicked AVIRIS reflectance data were used to build a mask excluding pixels with values of zero for every band in order to identify all pixels that contained data within the study area. Next, the DEM was masked using the AVIRIS-derived mask band, and subsequently layer stacked in ENVI beneath with the AVIRIS reflectance data.

4.3.3 VIPER Tools

4.3.3.1 Spectral Library Construction and Management

One important aspect of supervised classification methods is the construction of a library of training data; the classifier makes use of a subset of known values within the study area, such as the field-derived polygons, referred to as regions of interest (ROIs), for each class and extrapolates using these training values to the rest of the study area in order to classify the entire area. Each training pixel has a known field polygon-derived land cover class and associated spectral profile of AVIRIS-derived electromagnetic reflectance values, which are added to a spectral library. This spectral library is the best approximation of possible spectral profiles that each class will likely exhibit. Because the training pixels will not necessarily provide every possible spectral profile for a given land cover class, the classifier uses these training spectra in order to categorize pixels from the rest of the study area into the most likely land cover class. In order to aid in the accuracy of land cover classification, supplementary data such as DEMs can be concatenated, or

layer stacked, with AVIRIS data as an additional band. The utility of layer stacking a DEM with AVIRIS data is that the classifier will now take into account the elevations at which certain land cover classes occur, potentially preventing the inaccurate classification of a land cover class at an elevation that falls outside its normal range. VIPER Tools, an image analysis extension for ENVI, was used with the training polygons as ROIs to first build spectral libraries from layer-stacked AVIRIS and DEM data. Once the spectral library was constructed, it was sorted by vegetation class and redundant spectra were removed from the library with an IDL program.

4.3.3.2 Linear Discriminant Analysis

After constructing and removing redundancies from each spectral library, the LDA classification was executed using an IDL program that was run in ENVI 5.3 Classic + IDL.

4.3.4 Visual Assesssment

Upon completion of the classification process, the results were visually inspected for errors, accuracy, discontinuities, and artifacts. Generally, if there was a large discontinuity in the raw AVIRIS reflectance mosaic (such as BRDF effects between two flight lines), it was also present in the classified image as a north-south trending line, in the same location as the AVIRIS data suture with a different dominant vegetation class east and west of the line.

4.3.5 Accuracy Assessment

A postclassification confusion matrix was generated for each classified image result using the validation polygons as ground-truth ROIs to determine the accuracy of each LDA iteration. User's and Producer's accuracies as well as the kappa coefficient were used to compare classifications of the same year. From these results, the most accurate classifications for each year were identified and used in analysis to address the project's research objectives.

4.4 Fractional Cover Analysis

Zachary Tane of the USDA Forest Service provided fractional cover data generated through MESMA analysis of the same 2013-2015 AVIRIS dataset used for LDA in this study. These fractional cover data provided information on the relative proportion of GV, NPV, soil, and shade for each pixel in the study area.

4.4.1 Shade Normalization

In order to quantify vegetation response for the study period, a normalization operation was applied to the fractional cover data for each year. Shade normalization excludes shade as a fractional cover endmember, and normalizes the remainder of non-shade endmembers on a scale from 0 to 1. The following equation is applied to each fractional cover endmember for each pixel analyzed:

$$Shade\ Normalized\ (EM_i) = \frac{EM_i}{EM_i + EM_{i+1} + EM_{i+2}}$$

EM denotes a non-shade endmember (i.e., GV, NPV, or soil) and the ratio of each non-shade endmember to the sum of all non-shade endmembers is equivalent to the shade

normalized value for an endmember. This process eliminates variation in canopy shade effects, but is still subject to the same BRDF effects that affect other classification methods such as LDA.

4.4.2 General GV, NPV, and Soil Analysis

Before analyzing the changes in either GV, NPV, or soil, an overall assessment of the relative values for each endmember across the study area was conducted in order to contextualize the analysis. Each endmember fraction was mapped individually to determine zones of relative abundance and scarcity, and to identify any artifacts that were related to BRDF effects. The goal of utilizing the fractional cover in analysis was to determine which endmember, if any, was representative of vegetation changes that were occurring as a response to increasing drought severity in the landscape. Thus GV, NPV, and soil were compared against one another for each year and between years.

4.4.2.1 GV Changes as Vegetation Response Indicator

Using the field-derived polygon areas as a sample subset of the entire study area, GV, NPV, and soil fractional cover were analyzed to determine general trends from 2013 to 2015. All vegetated land cover class polygons (HC, LC, MD, and MO) experienced a decreasing fraction of GV and increasing fraction of soil (Figure 6). NPV for all vegetated land cover class polygons did not experience a measureable increase or decrease. When vegetation mortality begins to occur, GV will first covert to NPV, and then into soil. From 2013-2014 and 2014-2015, no measureable increase in NPV was observed in the field derived polygons' fractional cover.

However, an increase in soil fractional cover was observed. NPV and soil have similar spectral profiles and are more similar spectrally than either NPV or soil is to GV. It was determined that inexplicably high variations in NPV and soil were present in the fractional cover data from 2013 to 2015 that could not necessarily be attributed to a reasonable physical vegetation change. Because it was not possible to independently verify the accuracy of the NPV and soil fractional cover results (i.e., whether NPV did or did not increase from 2013 to 2015), most reliable indication of vegetation response was determined to be GV and was used to quantify mortality. Change in GV showed a statistical, negative trend from 2013 to 2015, which could represent a vegetation response to increasing drought severity. Thus, GV was the only endmember identified as an indicator of vegetation response within the study area and was analyzed to determine degree of vegetation response to drought.

4.4.3 GV Changes by Vegetation Class

Using the field-derived land cover polygons, each vegetation class was analyzed for changes in GV in order to determine which classes experienced the strongest change. These changes in GV for each class were interpreted as vegetation potentially responding to intensifying drought conditions in the landscape. Thus, analysis of vegetation response to drought by vegetation class was quantified.

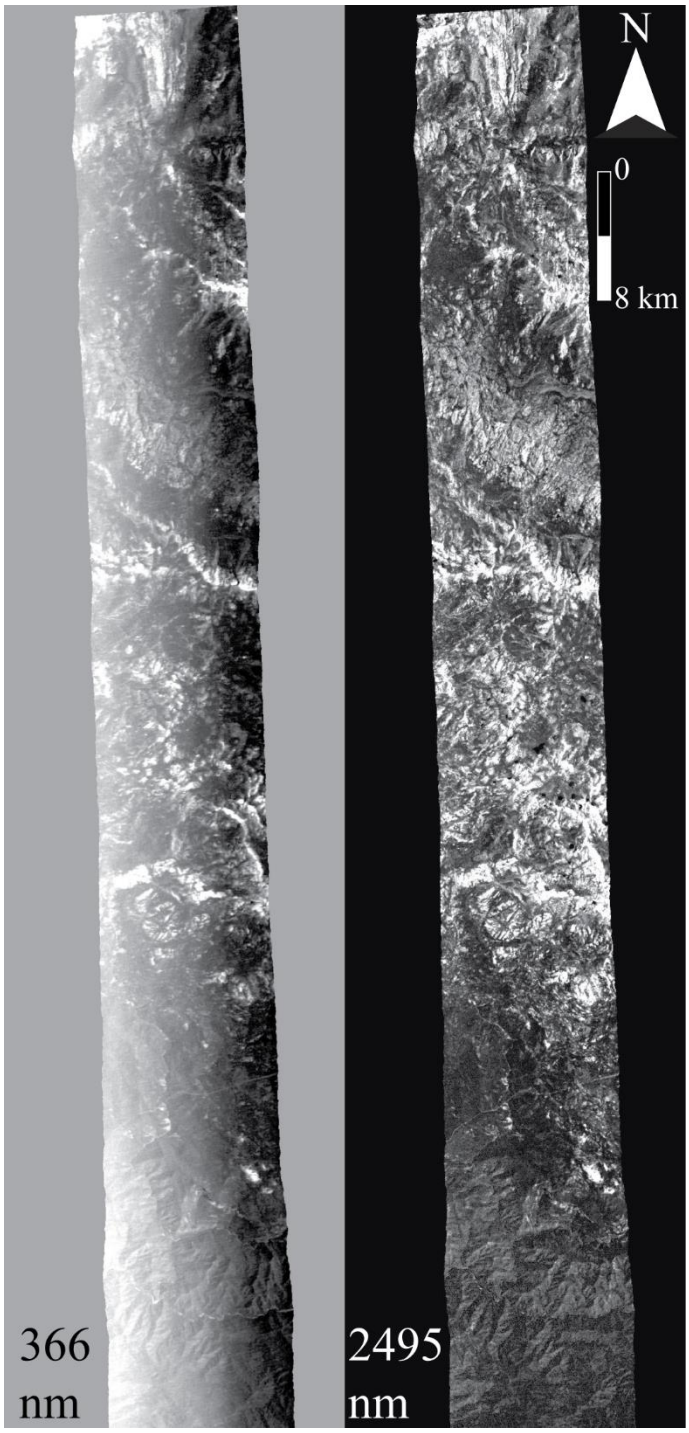

Figure 5. BRDF effects are present in many flight lines, an example is presented: Flight line 3 of 2013 AVIRIS reflectance data. Solar zenith angle is 51.37 degrees and solar azimuth is 99.45 degrees (illumination is just south of east). **A)** Band 1 (~366 nm) displays backscattering on the west side of the image and shadows on the east, consistent with BRDF effects as the sensor swept back and forth in an east-west trend. **B)** Band 224 (~2495 nm) displays very weak if any BRDF effects, which illustrates the wavelength-dependent nature of backscattering and shadows.

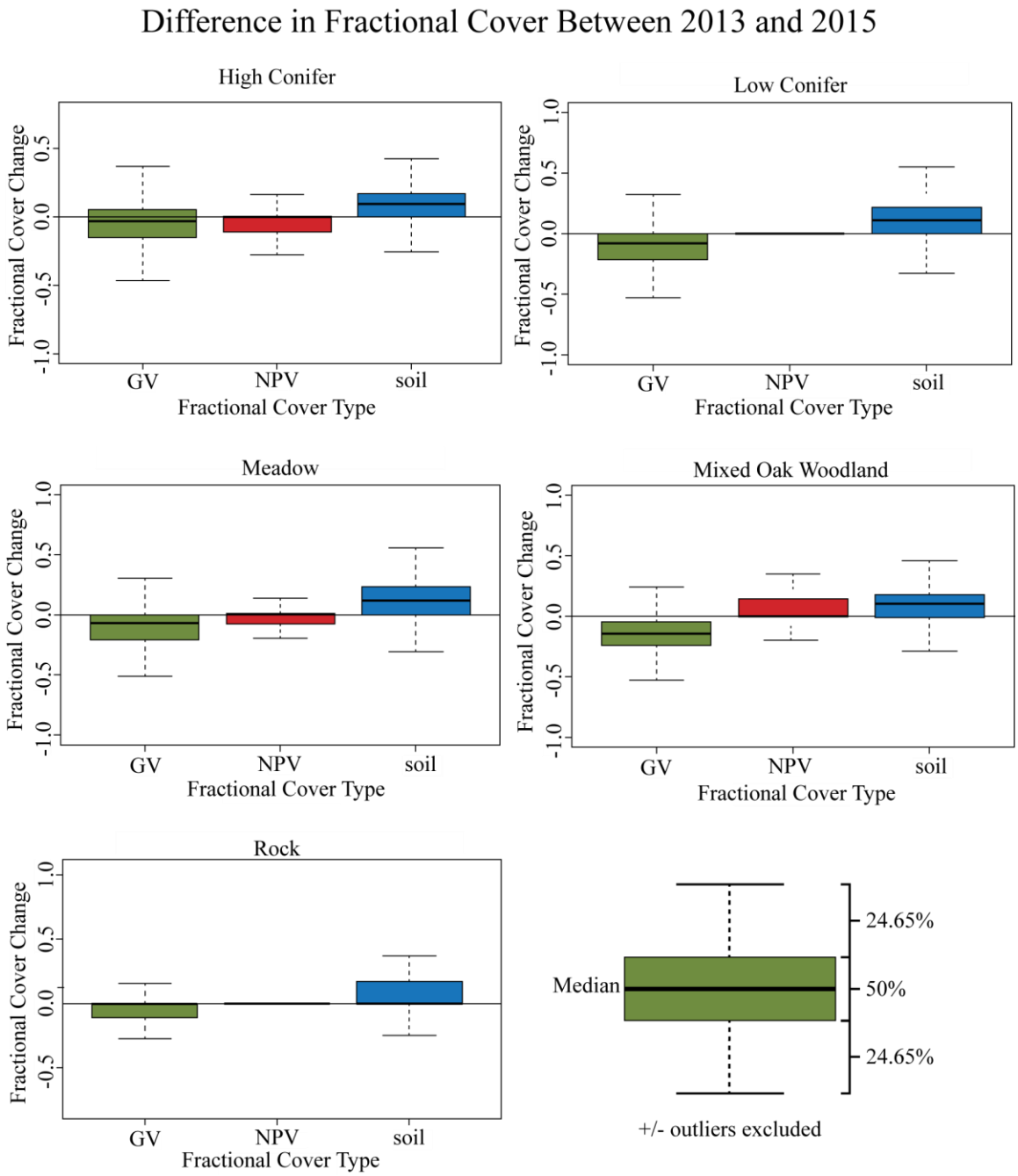

Figure 6. Boxplots of land cover class polygons' fractional cover difference between 2013 and 2015. Note that soil shows an increase across all vegetation classes, GV shows a decrease, and NPV shows no measurable change. The expected result of a decrease in GV is an increase in NPV, which was not observed, indicating the possibility that NPV was mistaken for soil, or alternatively that the conversion rate of GV into NPV was equal to the conversion rate of NPV to soil.

CHAPTER 5

RESULTS

5.1 Linear Discriminant Analysis

Classification of land cover from AVIRIS data decreased in overall accuracy from 2013-2015 (Table 3). The maximum overall classification accuracy and kappa coefficient obtained for each year's data was used as a metric to compare accuracies from 2013 to 2015. Overall classification accuracy was greatest in 2013 at 88.0%, lower in 2014 at 84.1%, and lowest in 2015 at 81.4%. The trend in associated kappa coefficients for each year also decreased from 2013 to 2015.

These decreasing accuracies may have resulted from increasing vegetation response to intensifying drought conditions that act to minimize the separability of vegetation land cover classes. However, strong BRDF effects present in AVIRIS data may have decreased the between-class separability of vegetation land cover in the same manner as vegetation response to drought. Therefore, while it does appear that stronger drought conditions are associated with lower classification accuracies, this conclusion cannot be confirmed in this study without eliminating the strong BRDF effects present in the AVIRIS data.

LDA classification maps (Figure 7) vary drastically in degree of spatial discontinuities and vegetation class occurrence in the landscape. The classified map of

vegetation land cover associated with highest LDA classification accuracy obtained from the 2013 data has obvious north-south trending discontinuities explained by changes in reflectance caused by differences in BRDF along each flight line. In addition, the 2013 map may also reflect over-classification of the high conifer and meadow classes. Discontinuities present within the 2014 classified map are more numerous and more pervasive throughout the study area than the 2013 classified image. However, classification accuracy results from 2015, which were lower than any other year, seem to have fewer discontinuities and misclassified regions: even fewer than 2013, despite the lower overall classification accuracy. The land cover classified map derived from 2013 AVIRIS data appears to have a limited number of both BRDF-related classification artifacts and misclassified regions.

5.2 Fractional Cover Analysis

5.2.1 GV Changes by Land Cover Class

Field-derived polygons were used as ROIs to examine changes in fractional cover for all land cover classes. Because these polygons are associated with known homogeneous land cover classes, the statistics derived from these regions can be utilized with confidence; these pixels analyzed for a given class only represented that class, whereas pixels from classified image results may not have truly represented the assigned class. Because GV was used as a metric to determine degree of vegetation response to drought conditions, the time-respective increase or decrease in fractional cover for GV of each vegetation class was compared to every other class. Median values for GV change across the study period are reported in Table 4 and illustrate that mixed oak (mo)

experienced greater decreases in fractional cover of GV than other vegetation classes, such as high conifer (hc). Table 4 also indicates that the majority of GV change that occurred for each vegetation class took place from 2013 to 2014, and that there was negligible change for classes from 2014 to 2015.

Of the vegetated land cover classes, the period and class associated with greatest GV change was mixed oak from 2013-2014, while the period and class associated with the least change was high conifer from 2013-2015. Figure 8 offers a graphical representation of GV changes by vegetation class and highlights the unequal GV changes associated with each vegetation class.

A closer examinination of which classes exhibited the greatest vegetation response to drought was conducted by examining land cover classes by GV change quartile breaks (Figure 9). These data were only collected from field-polygons that were not fire-affected. The first quartile, which included pixels with the greatest GV decrease, was dominated by mixed oak and low conifer. Because the number of pixels varied for each land cover type, each class was individually compared to itself between quartiles to determine the degree and range of its GV change.

Mixed oak and low conifer dominate the quartile of greatest GV decrease, but because mixed oak has a smaller number of pixels in the other quartiles and low conifer has a large number of pixels in all quartiles, it is reasonable to assume that mixed oak experienced a more significant loss of GV than low conifer.

Spatially, the regions of greatest GV decrease were generally located in the southwestern side of the study area, though there was GV decrease present throughout the entire region (Figure 10). BRDF effects may have affected fractional land cover values,

which is evident along flight line boundaries. There are also two areas of strong localized GV decrease, one in the center of the study area, and one to the northwest, both of which are areas associated with fires. These extreme GV loss areas serve as a basis of comparison to which the rest of the study area can be related. In the areas burned by fire, GV change values were much more extreme, and some pixels experienced 100% loss of GV. The majority of the study area not affected by fire still experienced a negative change in GV of ~6%. This suggests that the entire area reflected vegetation response to persistent drought conditions.

5.2.2 GV Changes by Elevation Bin

Given that drought conditions were persistent throughout the study area, the fact that some areas in the landscape experienced greater loss of GV than others necessitated an examination of another factor such as elevation. Using the same GV quartile ranges, elevation intervals were examined for their relationship to loss of GV. Figure 11 illustrates that the quartile of greatest GV decrease was dominated by the two lowest elevation ranges, such that the lower two elevation intervals are expressed more in the first and second quartiles of greatest GV decrease than the higher elevation intervals. Because all fire affected polygons were removed from analysis, there no fire-induced bias of GV loss present in any class.

5.3 Discussion

This study tested whether drought-induced vegetation response could be measured via decreases in GV, if GV decreases were more pronounced at lower

elevations, and thus whether forest ecosystems at lower elevations had a greater vegetation response to drought than those at higher elevations. This was done by classifying hyperspectral data into both discrete land cover classes based on dominant flora and bedrock, and into fractional cover classes as a function of photosynthetic capacity of vegetation. Secondary to this was whether the accuracies of classification methods were affected by intensifying drought conditions.

Mixed oak, more than any other vegetation class, experienced a strong decrease in fractional cover of GV (16%) within the field polygons analyzed. Likewise, low elevation regions from 695-1904 m (2280-6247 ft) in the landscape experienced a greater decrease in GV compared to higher elevation areas from 1904-2779 m (6247-9117 ft). Given that mixed oak was classified more in low elevation areas than other classes, these results indicate that the areas of greatest vegetation response to drought conditions were likely low elevation areas dominated by mixed oak vegetation. These results also indicate that low conifer experienced a decrease in GV (6%), even when accounting for pixel decreases due to fire. Every vegetated land cover class in the study area experienced varying degrees of vegetation response to drought conditions as evidenced by overall negative changes in GV for each class.

The timing and severity of drought-induced vegetation mortality can be affected by both current and past droughts, leading to delayed mortality in some cases (Bigler et al., 2007). Therefore, mortality as measured by GV loss in this study is likely affected to some degree by past drought periods in addition to the drought conditions present from 2013-2015. The relative decrease of GV present across all vegetated land cover classes is likely due to disproportionate GV decreases among some taxa more than others. The

following analysis of vegetation based on the taxa found in Table 2 elucidates the most likely culprits of GV loss for each vegetated land cover class. A summary of drought tolerance for different species can be found in Figure 12.

5.3.1 Mixed Oak

Generally, mixed oak contains more deciduous vegetation than any other land cover class, which, depending on the timing of each deciduous taxon's senescence and leaf-drop, could affect GV values considerably (Figure 12). However, a number of these deciduous taxa in the mixed oak class are also highly drought resistant. Thus, less drought resistant perennials could be experiencing drought-induced senescence, contributing to GV loss. Based on drought tolerance and foliage-retention, the most likely culprits of GV loss in the mixed oak class would likely include interior live oak, California black oak, Jeffrey pine, woolly leaf ceanothus, Oregon oak, blue oak, and California buckeye. A wide variety of grasses grow throughout the Sierra Nevada, and are especially prevalent in the lower elevation mixed oak class. It is likely, given the evapotranspirative characteristics of grasses relative to shrubs and trees, that grass senescence contributed to loss of GV in mixed oak.

5.3.2 Low Conifer

Pharis (2010) suggests that ponderosa pine and incense cedar are more drought resistant compared to sugar pine, suggesting that among these three evergreen species, sugar pine is the most likely to experience GV loss and thus mortality-related senescence. Furthermore, this finding that sugar pine is contributing to GV loss in low conifer was

confirmed by field observations. Lodgepole pine is not drought-tolerant and thus is also likely to contribute to GV loss in the upper extent of the low conifer land cover class, although lodgepole pine is much more common in the high conifer class. Both ponderosa pine and Jeffrey pine become more susceptible to bark beetle infestations during times of drought-induced stress (Fettig et al., 2012). For example, while ponderosa pine may be relatively resistant to stress directly related to drought conditions, this stress increases the susceptibility of these trees to secondary stresses (i.e., bark beetle attacks and disease), which can induce mortality.

5.3.3 High Conifer

Lodgepole pine is common in the high conifer class along with red fir, which, like Lodgepole, lacks drought tolerance. This class contains monotypic stands of both taxa throughout. Additionally, there are occurrences of both ponderosa pine, which is drought tolerant and white fir, which is only moderately drought tolerant. Although this class experienced the least degree of GV loss (Table 4 and Figure 8), it is comprised of predominately non-drought-tolerant flora, suggesting that drought conditions were less severe in this class. Of the dominant flora present in high conifer, it is most likely that GV loss is attributable to lodgepole pine, red fir, and perhaps white fir.

5.3.4 Summary of Taxa Characteristics

Given that mixed oak had the greatest decrease in GV of any class at 16% (Figure 8) and also is comprised of the most drought-tolerant taxa, it is interesting to note that while both high conifer and low conifer experienced less GV decrease (5% and 6%,

respectively) than mixed oak, both of the conifer classes had fewer drought-tolerant taxa (Figure 12).

Loss of GV can occur either because of mortality-related senescence or due to late green-up. If for instance California buckeye, a deciduous tree, experiences green-up at roughly the same time each year, AVIRIS data collection is likely to consistently capture the same seasonal stage of the tree from year to year (e.g., pregreen-up GV, green-up GV, nominal GV). However, the possibility does exist that drought-induced stress may change the dates of seasonal green-up and senescence for deciduous flora enough to capture a non-mortality-related apparent loss of GV in AVIRIS data in subsequent years. Perennials like Jeffrey pine that are not highly drought tolerant and do not drop foliage could potentially be captured by AVIRIS data experiencing drought-induced mortality, which would result in a loss of GV. The measured decreases in GV for the vegetated classes are likely due to a combination of factors both mortality-related and seasonally-related.

Figure 12 shows that the mixed oak woodland class contains several deciduous taxa, the low conifer class only contains a single taxon, and the high conifer class contains none. Seasonally-related GV loss may be affecting the mixed oak woodland class, but is unlikely affecting either the low conifer or high conifer classes in a significant manner, because of the distribution of deciduous taxa in these forested classes. Figure 8 and Table 4 both indicate that significant changes in GV took place for high conifer and low conifer forests. It is likely that these GV decreases are linked to drought-related vegetation mortality because low conifer lacks deciduous vegetation and high conifer only includes one deciduous taxon. Vegetation mortality occurs through both

direct drought-induced senescence and indirect increased susceptibility to bark beetles attacks and disease. Since at least two vegetated classes did experience vegetation mortality, it is likely that mixed oak also experienced drought-related mortality in addition to seasonal shifts in deciduous green-up. Mixed oak includes more drought-tolerant taxa, which logically would be less affected by drought than the moderate to low tolerance taxa of the conifer classes (Figure 12). The degree to which seasonal green-up timing affected GV loss relative to mortality requires further analysis.

Low conifer shares taxa with both the mixed oak and high conifer classes and generally resides at elevations between mixed oak and high conifer elevations (Figure 13). Figure 8 shows that loss of GV for low conifer was on average more severe than high conifer, but less severe than mixed oak. This could indicate that the taxa which were shared between these classes had a normalizing effect on measured GV loss. Each shared taxon could have either contributed to GV loss or not, possibly depending on its elevation and/or topography (e.g., on a slope, in a valley, on a ridge, etc.). Because these shared taxa were present across classes, they may have acted to mitigate taxa-related differences in measured GV loss. Minimizing confounding variability, such as how two different taxa react to the same external stimuli, between classes adds a greater level of confidence to the results than if no taxa were shared between classes.

Besides the effects of deciduous vegetation on GV loss, the only remaining variable that was measured to be associated with GV loss was elevation. The majority of the mixed oak class resides at lower elevations than low conifer or high conifer. Figure 11 shows that lower elevation areas have on average greater GV loss than higher elevation areas. Elevation plays a strong role in determining which dominant flora are

present in a given area. Since mixed oak occupies a lower elevation range, it is difficult to determine whether the flora present in mixed oak had more of an impact on GV loss than elevation, as flora is determined in part by elevation.

GV loss occurred for all classes, including rock and meadow, which lack a significant number of trees. However, fractional data and subsequent analysis (Figure 8) indicate that both experienced a loss in GV. This was likely due to the presence of grasses and herbaceous growth in these classes. Grasses were likely present in all classes' polygons and had varying effects on GV loss for each class depending on the presence of shrubs and trees. The rock land cover class, whose vegetation is primarily limited to partial grasses, shrubs, and lichen covers, experienced a significant loss of GV (Figure 8). Other classes such as mixed oak woodland and meadow also show a decrease in GV that may be attributable to senescence or mortality of a variety of grass taxa, which are abundant within these land cover types.

Table 3. Summary of maximum accuracies attained via LDA classification of land cover classes.

	2013	2014	2015
Overall Accuracy (%)	88.0	84.1	81.4
Kappa Coefficient	0.83	0.77	0.73

Table 4. Summary of mean changes in GV by vegetation class using fractional cover values extracted from field-derived polygon pixels. Statistics were generated in RStudio.

	2013-2014	2014-2015	2013-2015
hc	-6%	1%	-5%
lc	-8%	1%	-6%
md	-10%	-1%	-11%
mo	-13%	-2%	-16%
ro	-3%	-4%	-7%

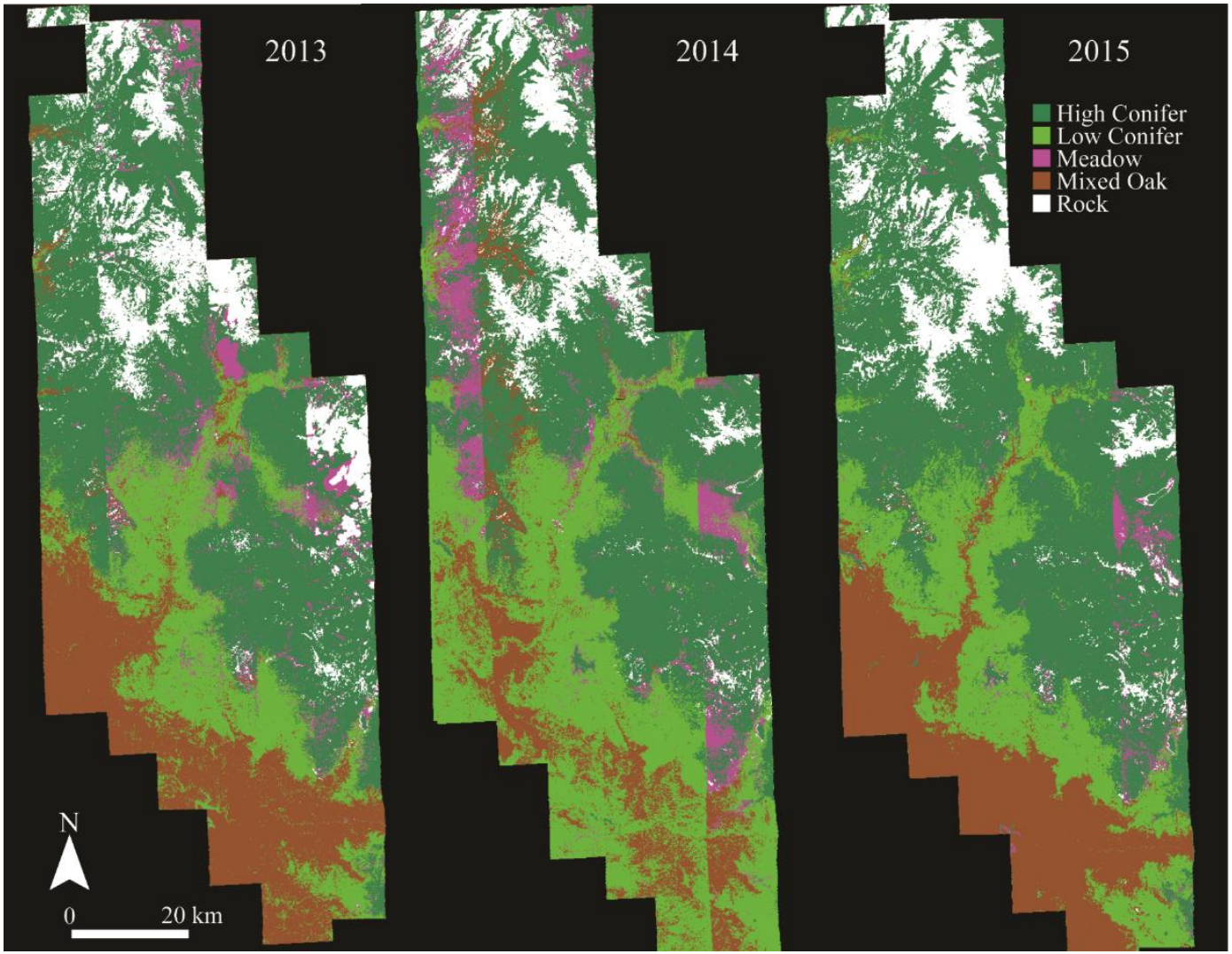

Figure 7. LDA classified image results of dominant land cover for 2013-2015. Linear artifacts are visible along flight line boundaries associated with strong BRDF effects.

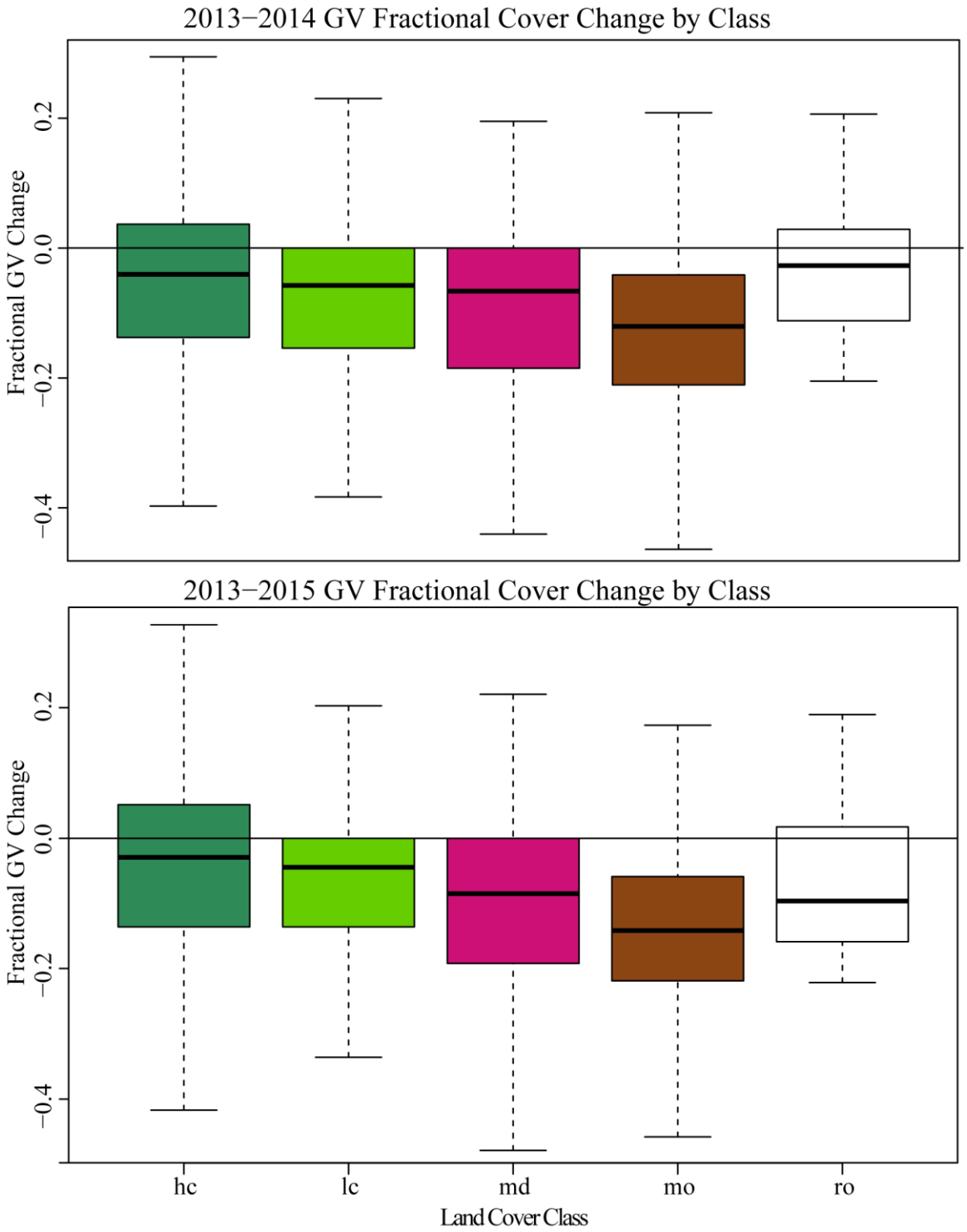

Figure 8. Median and quartile ranges of GV difference for vegetation classes computed from pixels within field-derived polygons. Note that each vegetation class experiences an overall decrease in GV fraction, with mixed oak (mo) having the greatest decrease in GV fractional cover.

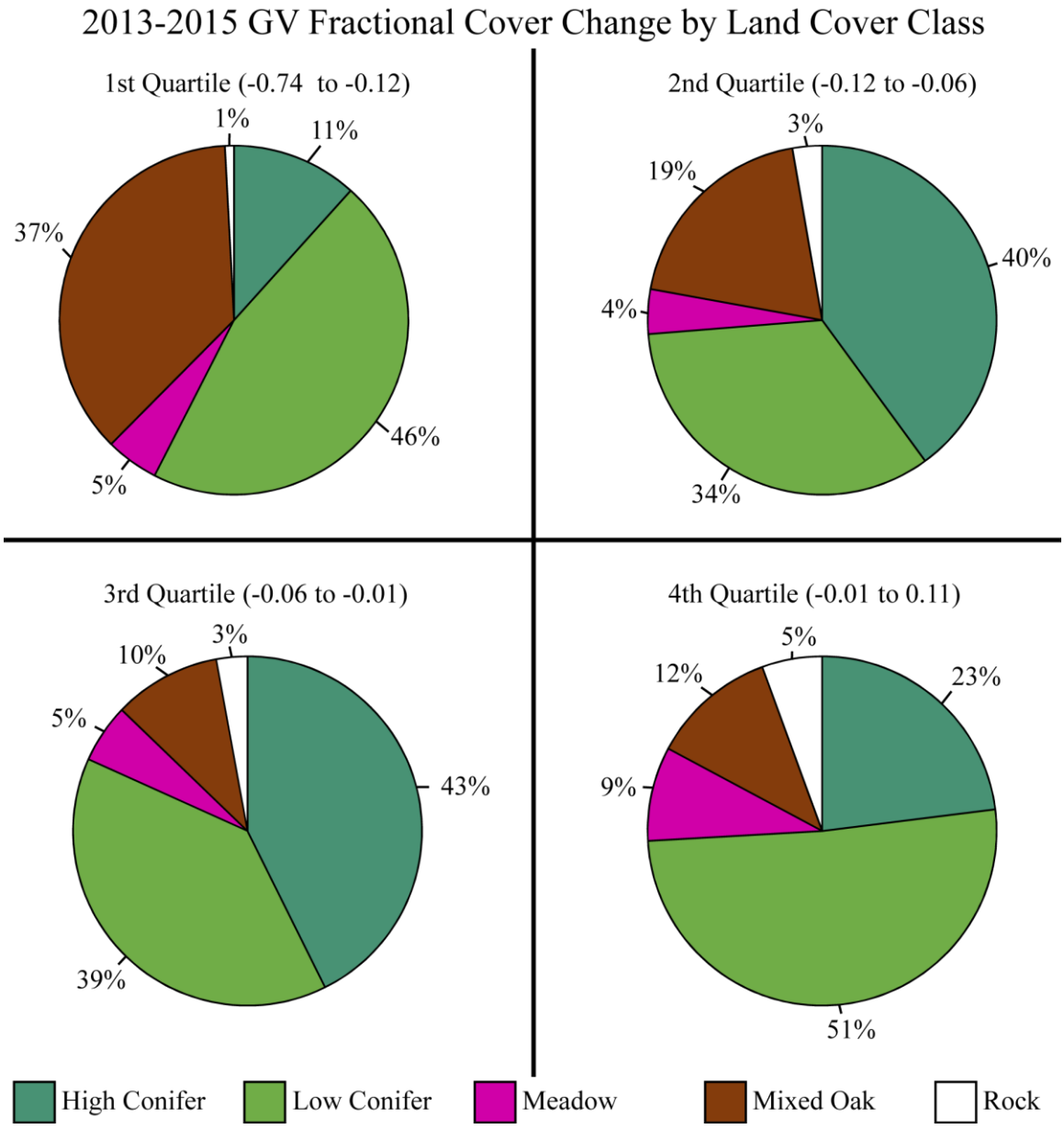

Figure 9. 2013-2015 GV difference quartiles plotted as pie charts with land cover classes. The majority of mixed oak's pixels fall into the lower percentile of GV difference, indicating this class experienced a greater decrease in GV than other classes.

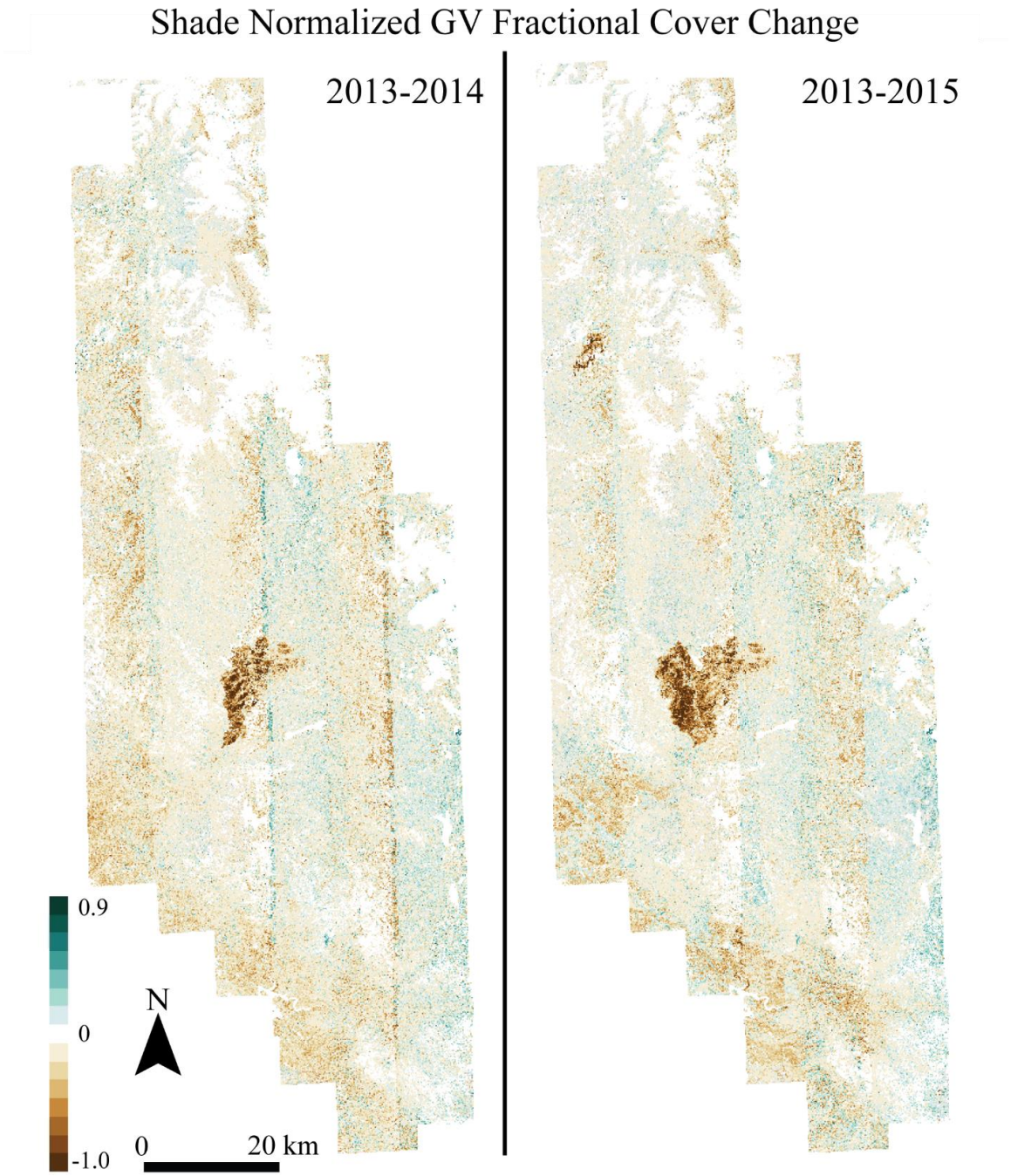

Figure 10. Shade normalized GV difference maps indicate that the southwestern region of the study area experienced greater decreases in GV than elsewhere. In July 2013, an area in the central region of the study area experienced a fire, the Aspen Fire, causing the large decrease in GV. Then, in August 2014 an area in the northwest experienced a fire, the Meadow Fire, causing a similar GV decrease. The GV decrease present in center of the 2013-2015 map that is west of the Aspen Fire is due to a subsequent fire, the French Fire (CalFire, 2017; MTBS, 2017).

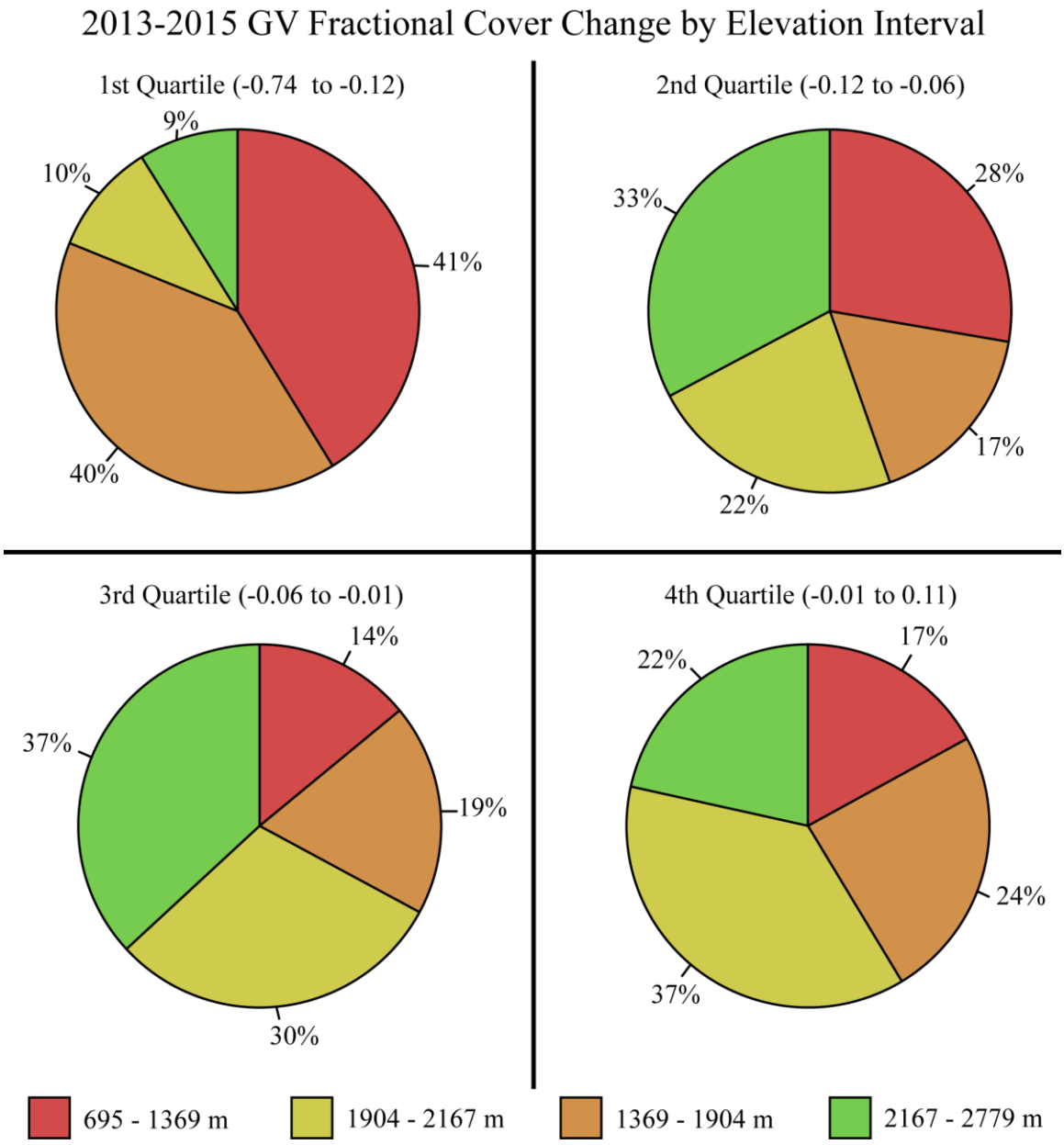

Figure 11**.** 2013-2015 GV difference quartiles plotted as pie charts with elevation intervals. Note that the lower elevations (695-1369 m and 1369-1904 m) express their greatest fractions in the 1st and 2nd quartiles while the higher elevation ranges dominated the 3rd and 4th quartile. This indicates that greatest loss of GV occurred more so at lower elevations than elsewhere in the landscape, and minimal GV loss up and GV increase occurred more so at higher elevations.

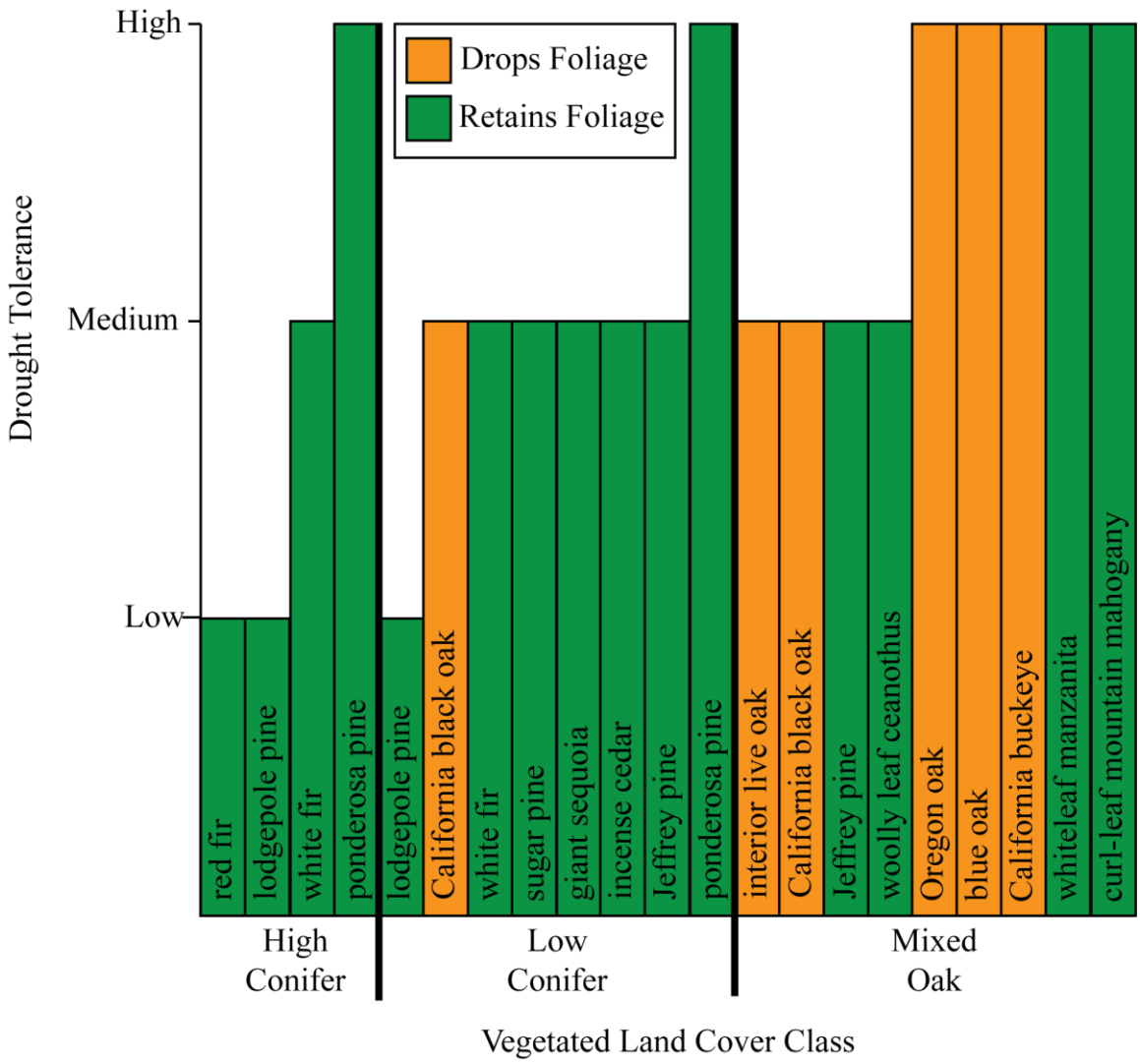

Figure 12. Taxa of each vegetated land cover class expressed as either retaining or dropping foliage annually and in terms of drought tolerance as enumerated by the USDA Natural Resource Conservation Service (CalFlora, 2017; USDA-NRCS, 2017). Note that mixed oak has on average a higher drought tolerance among taxa, and on average more deciduous taxa, while by contrast, high conifer has no deciduous taxa and fewer drought-tolerant taxa.

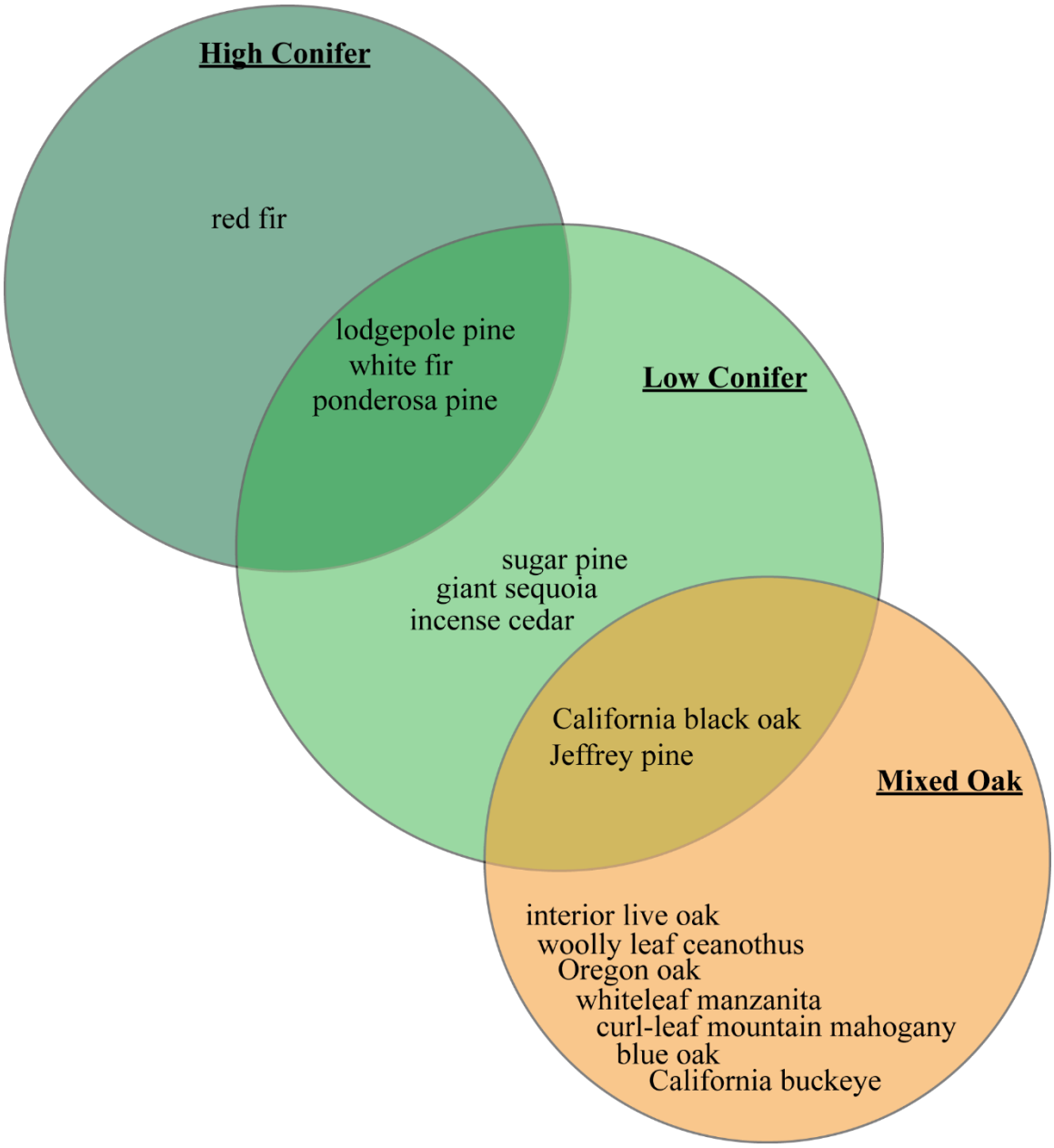

Figure 13. Venn diagram of taxa within each and between each vegetated land cover class. Note that low conifer shares taxa with both high conifer and mixed oak.

CHAPTER 6

CONCLUSION

6.1 Significance of Major Findings

Results from this study indicate that extensive drought-related mortality likely occurred in the central Sierra Nevada from 2013-2015. Decrease in GV fraction that may have been caused by mortality was measured across all land cover classes, but especially in the mixed oak woodland class with a GV loss of 16%, which could have been compounded by senescence for numerous deciduous taxa in this class. Elevation does seem to be predictive of GV loss to a degree, but this is also compounded by the elevation-dependence of certain taxa. Classification accuracy decreased over time as drought conditions persisted, possibly due to a drought-related reduction in the between-class separability of spectral profiles.

6.2 Strengths and Weaknesses of Study

6.2.1 Strengths

Field-derived polygons were physically delineated by ground-truthing homogeneous stands of dominant flora. These polygons allowed for the confident statistical treatment of MESMA fractional cover in order to elucidate trends between elevation, dominant flora composition, and between years. Determining classification

accuracies between years was only possible because of the availability and utilization of hyperspectral data for the same areas at roughly the same time of year across multiple, consecutive years. These hyperspectral data allowed for discrimination of vegetation classes using LDA, and is only possible at these taxa-scales with hyperspectral data, and not multispectral data.

6.2.2 Weaknesses

While consistent data collection at the same time of year aided in research goals, the lack of intra-annual data collection limited the degree to which seasonal vegetation changes could be measured to affect GV loss. This issue of determining whether changes in GV were related to mortality or senescence was hindered by the coarse time resolution available. Additionally, a more even distribution and greater number of field polygons across different regions in the study area would not only improve LDA classification analysis but also improve the robustness of land cover GV changes. Having polygons more widely dispersed across the landscape and in greater number would allow for more control over confounding variability such as topography, localized effects such as beetle attacks, and soil composition.

6.3 Suggested Future Analyses

6.3.1 Mortality vs. Senescence Analysis

Determining the degree to which deciduous vegetation experiences shifts in green-up and leaf fall is necessary in order to more accurately quantify the GV loss associated solely with drought-related mortality. Subsequent analyses should focus on

discerning between GV losses associated with drought-related senescence and time-shifts in seasonal foliage.

6.3.2 Intra-Annual Analysis

Data collection at various times of the year, including during winter months, would enable the study of postdrought recovery. The drought studied in this research was alleviated in the winter months of 2016, which would suggest that recovery would be measurable in the dates of green-up starting in 2017. By determining not only early summer fractional cover, but also early spring and winter, this would enable examination of time-series patterns related to current recovery and subsequent droughts. It would also help to determine if vegetation is able to recover at finer time scales throughout the year, instead of just between subsequent years. Additionally, comparing the relative timescales of recovery between megadroughts and shorter-lived droughts should be examined for a more holistic examination of forest recovery.

REFERENCES

Adams, J.B., Smith, M.O., Johnson, P.E., 1986. Spectral mixture modeling: A new analysis of rock and soil types at the Viking Lander 1 Site. J. Geophys. Res. 91, 8098. doi:10.1029/JB091iB08p08098

AghaKouchak, A., Cheng, L., Mazdiyasni, O., Farahmand, A., 2014. Global warming and changes in risk of concurrent climate extremes: Insights from the 2014 California drought. Geophys. Res. Lett. 41, 8847–8852. doi:10.1002/2014GL062308

Allen, C.D., Macalady, A.K., Chenchouni, H., Bachelet, D., McDowell, N., Vennetier, M., Kitzberger, T., Rigling, A., Breshears, D.D., Hogg, E.H.T., 2010. A global overview of drought and heat-induced tree mortality reveals emerging climate change risks for forests. For. Ecol. Manage. 259, 660–684.

Anderegg, W.R.L., Anderegg, L.D.L., Berry, J.A., Field, C.B., 2014. Loss of whole-tree hydraulic conductance during severe drought and multi-year forest die-off. Oecologia 175, 11–23. doi:10.1007/s00442-013-2875-5

Anderegg, W.R.L., Klein, T., Bartlett, M., Sack, L., Pellegrini, A.F.A., Choat, B., 2016a. Meta-analysis reveals that hydraulic traits explain cross-species patterns of drought-induced tree mortality across the globe. Pnas 113, 2–7. doi:10.1073/pnas.1525678113

Anderegg, W.R.L., Martinez-Vilalta, J., Cailleret, M., Camarero, J.J., Ewers, B.E., Galbraith, D., Gessler, A., Grote, R., Huang, C. ying, Levick, S.R., Powell, T.L., Rowland, L., S??nchez-Salguero, R., Trotsiuk, V., 2016b. When a tree dies in the forest: Scaling climate-driven tree mortality to ecosystem water and carbon fluxes. Ecosystems 19, 1133–1147. doi:10.1007/s10021-016-9982-1

Anderson, J.E., Plourde, L.C., Martin, M.E., Braswell, B.H., Smith, M.L., Dubayah, R.O., Hofton, M.A., Blair, J.B., 2008. Integrating waveform lidar with hyperspectral imagery for inventory of a northern temperate forest. Remote Sens. Environ. 112, 1856–1870. doi:10.1016/j.rse.2007.09.009

Anderson, R.S., Stillick Jr, R.D., 2013. 800 years of vegetation change, fire and human settlement in the Sierra Nevada of California, USA. Holocene 23, 823–832. doi:10.1177/0959683612471985

Asner, G.P., 1998. Biophysical and biochemical sources of variability in canopy reflectance. Remote Sens. Environ. 64, 234–253. doi:10.1016/S0034-4257(98)00014-5

Asner, G.P., Brodrick, P.G., Anderson, C.B., Vaughn, N., Knapp, D.E., Martin, R.E.,

2015. Progressive forest canopy water loss during the 2012–2015 California drought. Proc. Natl. Acad. Sci. 2015, 201523397. doi:10.1073/pnas.1523397113

Asner, G.P., Heidebrecht, K.B., 2002. Spectral unmixing of vegetation, soil and dry carbon cover in arid regions: comparing multispectral and hyperspectral observations. Int. J. Remote Sens. 23, 3939–3958. doi:10.1080/01431160110115960

Asner, G.P., Jones, M.O., Martin, R.E., Knapp, D.E., Hughes, R.F., 2008. Remote sensing of native and invasive species in Hawaiian forests. Remote Sens. Environ. 112, 1912–1926. doi:10.1016/j.rse.2007.02.043

Ault, T.R., Mankin, J., Cook, B.I., Smerdon, J.E., 2016. Relative impacts of mitigation, temperature, and precipitation on 21st-century megadrought risk in the American Southwest. Sci. Adv. 1–9.

Behmann, J., Steinrücken, J., Plümer, L., 2014. Detection of early plant stress responses in hyperspectral images. ISPRS J. Photogramm. Remote Sens. 93, 98–111. doi:10.1016/j.isprsjprs.2014.03.016

Beland, M., Roberts, D.A., Peterson, S.H., Biggs, T.W., Kokaly, R.F., Piazza, S., Roth, K.L., Khanna, S., Ustin, S.L., 2016. Mapping changing distributions of dominant species in oil-contaminated salt marshes of Louisiana using imaging spectroscopy. Remote Sens. Environ. 182, 192–207. doi:10.1016/j.rse.2016.04.024

Belmecheri, S., Babst, F., Wahl, E.R., Stahle, D.W., Trouet, V., 2016. Multi-century evaluation of Sierra Nevada snowpack. Nat. Clim. Chang. 6, 2–3. doi:10.1038/nclimate2809

Bigler, C., Gavin, D.G., Gunning, C., Veblen, T.T., 2007. Drought induces lagged tree mortality in a subalpine forest in the Rocky Mountains. Oikos 116, 1983–1994. doi:10.1111/j.2007.0030-1299.16034.x

Brunelle, A., Anderson, R.S., 2003. Sedimentary charcoal as an indicator of late-Holocene drought in the Sierra Nevada, California, and its relevance to the future. Holocene 13, 21–28. doi:10.1191/0959683603hl591rp

CalFire, 2017. California Statewide Fire Map [WWW Document]. URL http://www.fire.ca.gov/general/firemaps (accessed 1.8.17).

CalFlora, 2017. Search for Plants [WWW Document]. URL http://www.calflora.org/ (accessed 1.1.17).

Chen, J., Wang, R., Wang, C., 2008. A multiresolution spectral angle-based hyperspectral classification method. Int. J. Remote Sens. 29, 3159–3169. doi:10.1080/01431160701442138

Choat, B., Jansen, S., Brodribb, T.J., Cochard, H., Delzon, S., Bhaskar, R., Bucci, S.J., Feild, T.S., Gleason, S.M., Hacke, U.G., Jacobsen, A.L., Lens, F., Maherali, H., Martínez-Vilalta, J., Mayr, S., Mencuccini, M., Mitchell, P.J., Nardini, A., Pittermann, J., Pratt, R.B., Sperry, J.S., Westoby, M., Wright, I.J., Zanne, A.E., 2012. Global convergence in the vulnerability of forests to drought. Nature 4–8. doi:10.1038/nature11688

Coates, A.R., Dennison, P.E., Roberts, D.A., Roth, K.L., 2015. Monitoring the impacts of severe drought on southern California Chaparral species using hyperspectral and thermal infrared imagery. Remote Sens. 7, 14276–14291. doi:10.3390/rs71114276

Cochrane, M. a., 2000. Using vegetation reflectance variability for species level classification of hyperspectral data. Int. J. Remote Sens. 21, 2075–2087. doi:10.1080/01431160050021303

Cook, B.I., Ault, T.R., Smerdon, J.E., 2015. Unprecedented 21st century drought risk in the American Southwest and Central Plains. Sci. Adv. 1.

Cook, B.I., Smerdon, J.E., Seager, R., Cook, E.R., 2014. Pan-Continental Droughts in North America over the Last Millennium. J. Clim. 27, 383–397. doi:10.1175/JCLI-D-13-00100.1

Davis, O.K., Anderson, R.S., Fall, P.L., O'Rourke, M.K., Thompson, R.S., 1985. Palynological evidence for Early Holocene aridity in the southern Sierra Nevada, California. Quat. Res. 24, 322–332.

Davis, O.K., Moratto, M.J., 1988. Evidence for a warm dry Early Holocene in the western Sierra Nevada of California: Pollen and plant macrofossil analysis of Dinkey and Exchequer Meadows. Madrono 35, 132–149.

Dennison, P.E., Roberts, D.A., 2003a. The effects of vegetation phenology on endmember selection and species mapping in southern California chaparral. Remote Sens. Environ. 87, 295–309. doi:10.1016/j.rse.2003.07.001

Dennison, P.E., Roberts, D.A., 2003b. Endmember selection for multiple endmember spectral mixture analysis using endmember average RMSE. Remote Sens. Environ. 87, 123–135. doi:10.1016/S0034-4257(03)00135-4

Dolanc, C.R., Westfall, R.D., Safford, H.D., Thorne, J.H., Schwartz, M.W., 2013. Growth-climate relationships for six subalpine tree species in a Mediterranean climate. Can. J. For. Res. 43, 1114–1126. doi:10.1139/cjfr-2013-0196

Dudley, K.L., Dennison, P.E., Roth, K.L., Roberts, D.A., Coates, A.R., 2015. A multi-temporal spectral library approach for mapping vegetation species across spatial and temporal phenological gradients. Remote Sens. Environ. 167, 121–134. doi:10.1016/j.rse.2015.05.004

Elmore, A.J., Manning, S.J., Mustard, J.F., Craine, J.M., 2006. Decline in alkali meadow vegetation cover in California: The effects of groundwater extraction and drought. J. Appl. Ecol. 43, 770–779. doi:10.1111/j.1365-2664.2006.01197.x

Feret, J.-B., Asner, P.G., 2013. Tree Species Discrimination in Tropical Forests Using Airborne Imaging Spectroscopy. IEEE Trans. Geosci. Remote Sens. 51, 73–84. doi:10.1109/TGRS.2012.2199323

Fettig, C.J., Hayes, C.J., Jones, K.J., McKelvey, S.R., Mori, S.L., Smith, S.L., 2012. Thinning Jeffrey pine stands to reduce susceptibility to bark beetle infestations in California, U.S.A. Agric. For. Entomol. 14, 111–117. doi:10.1111/j.1461-9563.2011.00543.x

Fites-Kaufman, J., Rundel, P., Stephenson, N., Weixelman, D.A., 2007. Montane and subalpine vegetation of the Sierra Nevada and Cascade Ranges, in: Terrestrial Vegetation of California. pp. 456–501. doi:10.1525/california/9780520249554.003.0017

Fuchs, B., 2016. United States Drought Monitor [WWW Document]. Natl. Drought Mitig. Cent. Univ. Nebraska-Lincoln, U.S. Dep. Agric. Natl. Ocean. Atmos. Adm. URL www.droughtmonitor.unl.edu

Graumlich, L., 1991. Subalpine tree growth, climate, and increasing CO2 : An assessment of recent growth trends. Ecology 72, 1–11.

Green, R.O., Eastwood, M.L., Sarture, C.M., Chrien, T.G., Aronsson, M., Chippendale, B.J., Faust, J.A., Pavri, B.E., Chovit, C.J., Solis, M., Olah, M.R., Williams, O., 1998. Imaging spectroscopy and the Airborne Visible / Infrared Imaging Spectrometer (AVIRIS). Remote Sens. Environ. 227–248.

Heusser, L.E., Kirby, M.E., Nichols, J.E., 2015. Pollen-based evidence of extreme drought during the last Glacial (32.6-9.0 ka) in coastal southern California. Quat. Sci. Rev. 126, 242–253. doi:10.1016/j.quascirev.2015.08.029

Huang, C.Y., Anderegg, W.R.L., 2012. Large drought-induced aboveground live biomass losses in southern Rocky Mountain aspen forests. Glob. Chang. Biol. 18, 1016–1027. doi:10.1111/j.1365-2486.2011.02592.x

Johnson, E.W., Ross, J., 2008. Quantifying error in aerial survey data. Aust. For. 71, 216–222. doi:10.1080/00049158.2008.10675038

Keshava, N., Mustard, J.F., 2002. Spectral unmixing. IEEE Signal Process. Mag. 19, 44–57. doi:10.1109/79.974727

Kleppe, J.A., Brothers, D.S., Kent, G.M., Biondi, F., Jensen, S., Driscoll, N.W., 2011. Duration and severity of Medieval drought in the Lake Tahoe Basin. Quat. Sci. Rev. 30, 3269–3279. doi:10.1016/j.quascirev.2011.08.015

Kogan, F., Guo, W., 2015. 2006–2015 mega-drought in the western USA and its monitoring from space data. Geomatics, Nat. Hazards Risk. doi:10.1080/19475705.2015.1079265

le Maire, G., François, C., Soudani, K., Berveiller, D., Pontailler, J.Y., Bréda, N., Genet, H., Davi, H., Dufrêne, E., 2008. Calibration and validation of hyperspectral indices for the estimation of broadleaved forest leaf chlorophyll content, leaf mass per area, leaf area index and leaf canopy biomass. Remote Sens. Environ. 112, 3846–3864. doi:10.1016/j.rse.2008.06.005

Leung, L.R., Ghan, S.J., 1999. Pacific Northwest climate sensitivity simulated by a regional climate model driven by a GCM. Part II: 2 x CO^2 simulations. J. Clim. 12, 2031–2053. doi:10.1175/1520-0442(1999)012<2010:PNCSSB>2.0.CO;2

MacDonald, G.M., Kremenetski, K. V, Hidalgo, H.G., 2008. Southern California and the perfect drought: Simultaneous prolonged drought in southern California and the Sacramento and Colorado River systems. Quat. Int. 188, 11–23.

doi:10.1016/j.quaint.2007.06.027

Mao, Y., Nijssen, B., Lettenmaier, D.P., 2015. Is climate change implicated in the 2013-2014 California drought? A hydrologic perspective. Geophys. Res. Lett. 42, 2805–2813. doi:10.1002/2015GL063456

Meng, R., Dennison, P.E., Huang, C., Moritz, M.A., D'Antonio, C., 2015. Effects of fire severity and post-fire climate on short-term vegetation recovery of mixed-conifer and red fir forests in the Sierra Nevada Mountains of California. Remote Sens. Environ. 171, 311–325. doi:10.1016/j.rse.2015.10.024

Millar, C.I., King, J.C., Westfall, R.D., Alden, H.A., Delany, D.L., 2006. Late Holocene forest dynamics, volcanism, and climate change at Whitewing Mountain and San Joaquin Ridge, Mono County, Sierra Nevada, CA, USA. Quat. Res. 66, 273–287. doi:10.1016/j.yqres.2006.05.001

Miller, J.D., Safford, H.D., Crimmins, M., Thode, A.E., 2009. Quantitative evidence for increasing forest fire severity in the Sierra Nevada and southern Cascade Mountains, California and Nevada, USA. Ecosystems 12, 16–32. doi:10.1007/s10021-008-9201-9

Minckley, T.A., Bartlein, P.J., Whitlock, C., Shuman, B.N., Williams, J.W., Davis, O.K., 2008. Associations among modern pollen, vegetation, and climate in western North America. Quat. Sci. Rev. 27, 1962–1991. doi:10.1016/j.quascirev.2008.07.006

MTBS, 2017. Interactive Viewer - Monitoring Trends in Burn Severity [WWW Document]. URL https://www.mtbs.gov/viewer/index.html?region=all

NOAA, 2015. National Temperature Precipitation Maps: March 2015 Departure from Normal Temperature [WWW Document]. URL http://www.ncdc.noaa.gov/temp-and-precip/us-maps/1/201503?products[]=hprcc-mt#us-maps-select

Overpeck, J.T., 2013. The challenge of hot drought. Nature 503, 350–351. doi:10.1038/503350a

Panek, J., Saah, D., Esperanza, A., Bytnerowicz, A., Fraczek, W., Cisneros, R., 2013. Ozone distribution in remote ecologically vulnerable terrain of the southern Sierra Nevada, CA. Environ. Pollut. 182, 343–356. doi:10.1016/j.envpol.2013.07.028

Petel, A.M., 2005. Vegetation change across the late Pleistocene-Holocene transition in the Sierra Nevada, California, using pollen and stomate analysis. University of California, Los Angeles.

Pharis, R.P., 2010. Comparative drought resistance of five conifers and foliage moisture content as a viability index. Ecology 47, 211–221.

Roberts, D.A., Dennison, P.E., Roth, K.L., Dudley, K., Hulley, G., 2015. Relationships between dominant plant species, fractional cover and land surface temperature in a Mediterranean ecosystem. Remote Sens. Environ. 167, 152–167. doi:10.1016/j.rse.2015.01.026

Roberts, D.A., Gardner, M., Church, R., Ustin, S., Scheer, G., Green, R.O., 1998.

Mapping chaparral in the Santa Monica Mountains using multiple endmember spectral mixture models. Remote Sens. Environ. 65, 267–279. doi:10.1016/S0034-4257(98)00037-6

Roberts, D.A., Smith, M.O., Adams, J.B., 1993. Green vegetation, nonphotosynthetic vegetation, and soil in AVIRIS data. Remote Sens. Environ. V. 44, 255–269.

Robeson, S.M., 2015. Revisiting the recent California drought as an extreme value. Geophys. Res. Lett. 42, 6771–6779. doi:10.1002/2015GL064593

Roth, K.L., Roberts, D.A., Dennison, P.E., Alonzo, M., Peterson, S.H., Beland, M., 2015a. Differentiating plant species within and across diverse ecosystems with imaging spectroscopy. Remote Sens. Environ. 167, 135–151. doi:10.1016/j.rse.2015.05.007

Roth, K.L., Roberts, D.A., Dennison, P.E., Peterson, S.H., Alonzo, M., 2015b. The impact of spatial resolution on the classification of plant species and functional types within imaging spectrometer data. Remote Sens. Environ. 171, 45–57. doi:10.1016/j.rse.2015.10.004

Smith, S.J., Anderson, R.S., 1992. Late Wisconsin paleoecologic record from Swamp Lake, Yosemite National Park, California. Quat. Res. 38, 91–102. doi:10.1016/0033-5894(92)90032-E

Somers, B., Verbesselt, J., Ampe, E.M., Sims, N., Verstraeten, W.W., Coppin, P., 2010. Spectral mixture analysis to monitor defoliation in mixed-aged Eucalyptus globulus Labill plantations in southern Australia using Landsat 5-TM and EO-1 Hyperion data. ITC J. 12, 270–277. doi:10.1016/j.jag.2010.03.005

Stephenson, N.L., 1988. Climatic control of vegetation distribution: the role of the water-balance with examples from North America and Sequoia National Park, California. Ph.D. Thesis. Cornell University.

Stewart, I.T., Ficklin, D.L., Carrillo, C.A., McIntosh, R., 2015. 21st century increases in the likelihood of extreme hydrologic conditions for the mountainous basins of the Southwestern United States. J. Hydrol. 529, 340–353. doi:10.1016/j.jhydrol.2015.07.043

Street, J.H., Anderson, R.S., Paytan, A., 2012. An organic geochemical record of Sierra Nevada climate since the LGM from Swamp Lake, Yosemite. Quat. Sci. Rev. 40, 89–106. doi:10.1016/j.quascirev.2012.02.017

Tane, Z., 2016. Personal Communication.

Thenkabail, P.S., Enclona, E.A., Ashton, M.S., Legg, C., De Dieu, M.J., 2004a. Hyperion, IKONOS, ALI, and ETM+ sensors in the study of African rainforests. Remote Sens. Environ. 90, 23–43. doi:10.1016/j.rse.2003.11.018

Thenkabail, P.S., Enclona, E.A., Ashton, M.S., Van Der Meer, B., 2004b. Accuracy assessments of hyperspectral waveband performance for vegetation analysis applications. Remote Sens. Environ. 91, 354–376. doi:10.1016/j.rse.2004.03.013

Töpel, M., Antonelli, A., Yesson, C., Eriksen, B., 2012. Past climate change and plant evolution in western North America: A case study in Rosaceae. PLoS One 7. doi:10.1371/journal.pone.0050358

USDA-NRCS, 2017. Plants Database [WWW Document]. URL https://plants.usda.gov/java/ (accessed 1.1.17).

USDA Forest Service, 2016. Sierra Nevada Foothills, Transverse and Southern Coastal Ranges - Forest Health Protection Special Aerial Detection Survey.

Wathen, S.F., 2011. 1,800 Years of abrupt climate change, severe fire, and accelerated erosion, Sierra Nevada, California, USA. Clim. Change 108, 333–356. doi:10.1007/s10584-011-0046-4

Williams, A.P., Allen, C.D., Millar, C.I., Swetnam, T.W., Michaelsen, J., Still, C.J., Leavitt, S.W., 2010. Forest responses to increasing aridity and warmth in the southwestern United States. Proc. Natl. Acad. Sci. 107, 21289–21294. doi:10.1073/pnas.0914211107

Williams, A.P., Seager, R., Abatzoglou, J.T., Cook, B.I., Smerdon, J.E., Cook, E.R., 2015. Contribution of anthropogenic warming to California drought during 2012-2014. Geophys. Res. Lett. 42, 6819–6828. doi:10.1002/2015GL064924